INT. J. REMOTE SENSING, 20 MAY, 2004,
VOL. 25, NO. 10, 1893–1924

Taylor & Francis
Taylor & Francis Group

# Review article: Geometric processing of remote sensing images: models, algorithms and methods†

T. TOUTIN

Natural Resources Canada, Canada Centre for Remote Sensing, 588 Booth Street, Ottawa, Ontario, K1A 0Y7, Canada;
e-mail: thierry.toutin@ccrs.nrcan.gc.ca

(*Received 14 June 2002; in final form 18 December 2002*)

**Abstract.** The geometric processing of remote sensing images becomes a key issue in multi-source data integration, management and analysis for many geomatic applications. This paper first reviews the source of geometric distortions, compares the different mathematical models being currently used for geometric distortion modelling, details the algorithms, methods and processing steps and finally tracks the error propagation from the input to the final output data.

## 1. Introduction

Why ortho-rectify remote sensing images? Raw images usually contain such significant geometric distortions that they cannot be used directly with map base products in a geographic information system (GIS). Consequently, multi-source data integration (raster and vector) for applications in geomatics requires geometric and radiometric processing adapted to the nature and characteristics of the data in order to keep the best information from each image in the composite ortho-rectified products.

The processing of multi-source data can be based on the concept of 'terrain-geocoded images', a term originally invented in Canada in defining value-added products (Guertin and Shaw 1981). Photogrammetrists, however, prefer the term 'ortho-image' in referring to the unit of terrain-geocoded data, where all distortions including the relief are corrected. To integrate different data under the concept, each raw image must be separately converted to an ortho-image so that each component ortho-image of data set can be registered, compared, combined, etc, pixel by pixel but also with cartographic vector data in a GIS.

Why does the geometric correction process seem to be more important today than before? In 1972, the impact of the geometric distortions was quite negligible for different reasons:

†Revised and updated version of Chapter 6 in: *Remote Sensing of Forest Environments: Concepts and Case Studies*, M. A. Wulder and S. E. Franklin Editors, Kluwer Academic Publishers, Spring 2003.

*International Journal of Remote Sensing*
ISSN 0143-1161 print/ISSN 1366-5901 online 
http://www.tandf.co.uk/journals
DOI: 10.1080/0143116031000101611

- the images, such as Landsat-MSS, were nadir viewing and the resolution was coarse (around 80–100 m);
- the products, resulting from the image processing were analogue on paper;
- the interpretation of the final products was performed visually; and
- the fusion and integration of multi-source and multi-format data did not exist.

Now, the impact of distortions, although they are similar, is less negligible because:

- the images are off-nadir viewing and the resolution is fine (sub-metre level);
- the products resulting from image processing are fully digital;
- the interpretation of the final products is realized on computer;
- the fusion of multi-source images (different platforms and sensors) is in general use; and
- the integration of multi-format data (raster/vector) is a general tendency in geomatics.

One must admit that the new data, the method and processing, the resulting processed data, their analysis and interpretation introduced new needs and requirements for geometric corrections, due to a drastic evolution with large scientific and technology improvements between these two periods. Even if the literature is quite abundant mainly in terms of books and peer-reviewed articles (an exhaustive list is given in the references), it is important to update the problems and the solutions recently adopted for geometrically correcting remote sensing images with the latest developments and research studies from around the world. This review paper will then address:

- the source of geometric distortions and deformations with different categorizations (§2);
- the modelling of the distortions with different 2D/3D physical/empirical models and mathematical functions (§3); and
- the geometric correction method with the processing steps and errors (§4).

Comparisons between the models and mathematical functions, their applicability and their performance on different types of images (frame camera, visible infra-red (VIR) and infra-red oscillating or push-broom scanners; side looking antenna radar (SLAR) or synthetic aperture radar (SAR) sensors; high, medium or low resolution) are also addressed. The errors with their propagation from the input data to the final results are also evaluated through the full processing steps.

## 2. Sources of geometric distortions

Each image acquisition system (figure 1) produces unique geometric distortions in its raw images and consequently the geometry of these images does not correspond to the terrain or of course to a specific map projection of end-users. Obviously, the geometric distortions vary considerably with different factors such as the platform (aircraft versus satellite), the sensor (VIR or SAR; low to high resolution), and also the total field of view. However, it is possible to make general categorizations of these distortions.

The sources of distortion can be grouped into two broad categories: the *observer* or the acquisition system (platform, imaging sensor and other measuring instruments, such as gyroscope, stellar sensors, etc) and the *observed* (atmosphere and Earth). In addition to these distortions, the deformations related to the map

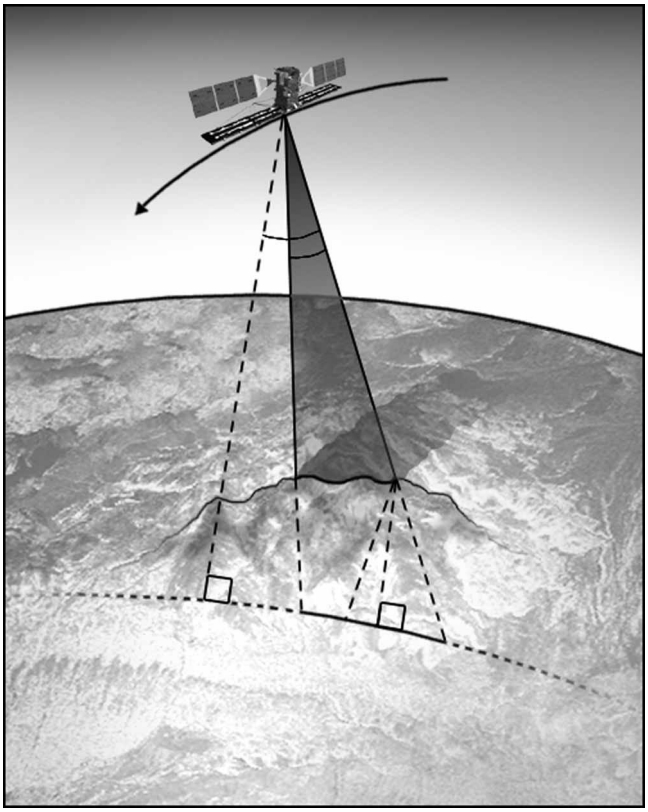

Figure 1. Geometry of viewing of a satellite scanner in orbit around the Earth.

projection have to be taken into account because the terrain and most GIS end-user applications are generally represented and performed respectively in a topographic space and not in the geoid or a referenced ellipsoid. Table 1 describes in more detail the sources of distortion for each category and sub-category. Figures 1 and 2 illustrate the geometry of acquisition and the quasi-polar elliptical orbit approximation of remote sensing satellites around the Earth, respectively. The map deformations are logically included in the distortions of the *observed*.

Previous studies made a second-level categorization into low, medium and high frequency distortions (Friedmann *et al*. 1983), where 'frequency' is determined or compared to the image acquisition time. Examples of low, medium and high frequency distortions are orbit variations, Earth rotation, and local topographic effects, respectively. While this categorization was suitable in the 1980s when there were very few remote sensing systems, today, with so many different acquisition systems, it is no longer acceptable because it differs with each acquisition system. For example, attitude variations are a high-frequency distortion for Quickbird or airborne push-broom scanner, a medium-frequency distortion for SPOT-HRV and Landsat-ETM$^+$ or a low-frequency distortion for Landsat-MSS.

The geometric distortions of table 1 are predictable or systematic and generally well understood. Some of these distortions, especially those related to the instrumentation, are generally corrected at ground receiving stations or by image vendors. Others, for example those related to the atmosphere, are not taken into

Table 1. Description of error sources for the two categories, the *observer* and the *observed*, with the different sub-categories.

| Category | Sub-category | Description of error sources |
|---|---|---|
| The *observer* or the acquisition system | Platform (spaceborne or airborne) | Variation of the movement<br>Variation in platform attitude (low to high frequencies) |
| | Sensor (VIR, SAR or HR) | Variation in sensor mechanics (scan rate, scanning velocity, etc)<br>Viewing/look angles<br>Panoramic effect with field of view |
| | Measuring instruments | Time-variations or drift<br>Clock synchronicity |
| The *observed* | Atmosphere | Refraction and turbulence |
| | Earth | Curvature, rotation, topographic effect |
| | Map | Geoid to ellipsoid<br>Ellipsoid to map |

account and corrected because they are specific to each acquisition time and location and information on the atmosphere is rarely available. They also are negligible for low-to-medium resolution images.

The remaining distortions associated with the platform (figure 2) are mainly orbit and Earth related (quasi-elliptic movement, Earth gravity, shape and movement) (Escobal 1965, Centre National d'Études Spatiales 1980, Light *et al*. 1980). Depending on the acquisition time and the size of the image the orbital perturbations have a range of distortions. Some effects include:

- platform altitude variation in combination with sensor focal length, the Earth's flatness and terrestrial relief can change the pixel spacing;
- platform attitude variation (roll, pitch and yaw) can change the orientation and the shape of VIR images; it does not affect SAR image geometry; and
- platform velocity variations can change the line spacing or create line gaps/overlaps.

The remaining sensor-related distortions include:

- calibration parameter uncertainty such as in the focal length and the instantaneous field of view (IFOV) for VIR sensors or the range gate delay (timing) for SAR sensors; and
- panoramic distortion in combination with the oblique-viewing system, Earth curvature and topographic relief changes the ground pixel sampling along the column.

The remaining Earth-related distortions include (figure 1):

- rotation, which generates latitude-dependent displacements between image lines;
- curvature, which for large width image creates variation in the pixel spacing; and
- topographic relief, which generates a parallax in the scanner direction.

The remaining deformations associated with the map projection are:

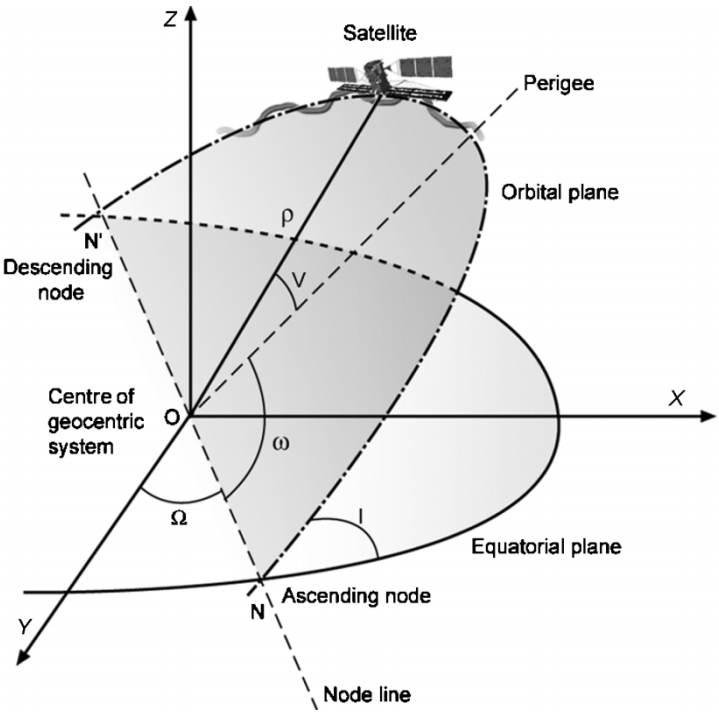


Figure 2. Description of a satellite orbit and its approximation by an ellipse. *XYZ* are the geocentric frame reference system. Ω is the longitude of the ascending node (N); $\omega$ is the argument of the perigee (P); $(\omega + v)$ is the argument of the satellite; $\rho$ is the distance from the Earth centre (O) and the satellite.

- the approximation of the geoid by a reference ellipsoid; and
- the projection of the reference ellipsoid on a tangent plane.

## 3. Geometric modelling of distortions

All these remaining geometric distortions require models and mathematical functions to perform geometric corrections of imagery: either through 2D/3D empirical models (such as 2D/3D polynomial or 3D rational functions, RFs) or with rigorous 2D/3D physical and deterministic models. With 2D/3D physical models, which reflect the physical reality of the viewing geometry (platform, sensor, Earth and sometimes map projection), geometric correction can be performed step-by-step with a mathematical function for each distortion/deformation, or simultaneously with a 'combined' mathematical function. The step-by-step solution is generally applied at the ground receiving station when the image distributors sell added-value products (georeferenced, map oriented or geocoded) while the end users generally use and prefer the 'combined' solution.

### 3.1. *2D/3D empirical models*

The 2D/3D empirical models can be used when the parameters of the acquisition systems or a rigorous 3D physical model are not available. Since they do not reflect the source of distortions described previously, these models do not

require *a priori* information on any component of the total system (platform, sensor, Earth and map projection).

These empirical models are based on different mathematical functions:

- 2D polynomial functions, such as:

$$P_{2D}(XY) = \sum_{i=o}^{m} \sum_{j=o}^{n} a_{ij} X^i Y^j \tag{1}$$

- 3D polynomial functions, such as:

$$P_{3D}(XYZ) = \sum_{i=o}^{m} \sum_{j=o}^{n} \sum_{k=o}^{p} a_{ijk} X^i Y^j Z^k \tag{2}$$

- 3D RFs, such as:

$$R_{3D}(XYZ) = \frac{\sum_{i=o}^{m} \sum_{j=o}^{n} \sum_{k=o}^{p} a_{ijk} X^i Y^j Z^k}{\sum_{i=o}^{m} \sum_{j=o}^{n} \sum_{k=o}^{p} b_{ijk} X^i Y^j Z^k}, \tag{3}$$

where: $X$, $Y$, $Z$ are the terrain or cartographic coordinates; $i$, $j$, $k$ are integer increments; and $m$, $n$ and $p$ are integer values, generally comprised between 0 and 3, with $m+n(+p)$ being the order of the polynomial functions, generally three.

Each 2D 1st, 2nd and 3rd order polynomial function will then have 3-, 6- and 10-term unknowns. Each 3D 1st, 2nd and 3rd order polynomial function will then have 4-, 10- and 20-term unknowns. The 2D/3D 1st order polynomial functions are also called affine transformations. Each 3D 1st, 2nd and 3rd order RF will have 8-, 20- and 40-term unknowns. In fact, the 3D RFs are extensions of the co-linearity equations (§3.3), which are equivalent to 3D 1st order RFs. Depending on the imaging geometry in each axis (flight and scan), the order of polynomial functions (numerator and denominator) can be different and/or specific terms, such as $XY^2$ for 2D or $XZ$, $YZ^2$ or $Z^3$, etc for 3D, and can be differently dropped of the polynomial functions, when these terms cannot be related to any physical element of the image acquisition geometry. These 'intelligent' polynomial functions better reflect the geometry in both axes and reduce the over-parameterization and the correlation between terms. Okamoto (1981, 1988) already applied this reduction of terms for one-dimensional central perspective photographs and line-scanners, respectively.

### 3.1.1. *2D Polynomial functions*

Since the 2D polynomial functions, with their formulation, are well known and have been documented since the 1970s (Wong 1975, Billingsley 1983), only a few characteristics are given. The polynomial functions of the 1st order (six terms) allow for only correcting a translation in both axes, a rotation, scaling in both axes and an obliquity. The polynomial functions of the 2nd order (12 terms) allow for correction, in addition to the previous parameters, torsion and convexity in both axes. The polynomial function of the 3rd order (20 terms) allows for correction of the same distortions as a 2nd order polynomial function with others, which do not necessarily correspond to any physical reality of the image acquisition system. In

fact, previous research studies demonstrated that 3rd order polynomial functions introduce errors in the relative pixel positioning in ortho-images, such as Landsat-TM or SPOT-HRV (Caloz and Collet 2001) as well as in geocoding and integrating multi-sensor images, such as SPOT-HRV and airborne SAR (Toutin 1995a).

Since the 2D polynomial functions do not reflect the sources of distortion during the image formation and do not correct for terrain relief distortions, they are limited to images with few or small distortions, such as nadir-viewing images, systematically-corrected images and/or small images over flat terrain (Bannari *et al.* 1995). Since these functions correct for local distortions at the ground control point (GCP) location they are very sensitive to input errors and hence GCPs have to be numerous and regularly distributed (Leeuw *et al.* 1988). Consequently, these functions should not be used when precise geometric positioning is required for multi-source/multi-format data integration and in high relief areas.

The 2D polynomial functions, as the simplest solution, were mainly used until the 1980s on images whose systematic distortions, excluding the relief, had already been corrected for by the image providers. As reported by Wong (1975), 2D 4th order polynomial functions were theoretically valid for low-resolution ERTS-1 imagery to approximate a rigorous 2D physical model (Kratky 1971). Extensions to conformal/orthogonal polynomial functions (Wong 1975, Leeuw *et al.* 1988) and surface-spline functions (Goshtasby 1988) were also used for Landsat-MSS. As mentioned in §1, good geometric accuracy was not a key factor in the analysis of analogue images, for which 2D polynomial functions could be appropriated. More recently, simple affine and projective functions applied to IKONOS Geo images (Hanley and Fraser 2001) or hybrid and projective functions to IKONOS Geo and IRS-1C images (Valadan Zoej *et al.* 2002) achieved good results because the images were acquired with near-nadir viewing angles over a flat terrain. However, while it is now known that 2D polynomial functions are not suitable regardless the image type and size as well as the terrain relief, some users still apply them, apparently without knowing the implications for subsequent processing operations and resulting digital products.

#### 3.1.2. *3D polynomial functions*

The 3D polynomial functions are an extension of the 2D polynomial function by adding $Z$-terms related to the third dimension of the terrain. However, they are prone to the same problems as any empirical functions, except for the relief: i.e. they are applicable to small images, they need numerous, regularly distributed GCPs, they correct locally at GCPs, they are very sensitive to errors, and they have a lack of robustness and consistency in the operational environment. Their use should be thus limited to small images or to systematically corrected images, where all distortions except the relief have been pre-corrected. For these reasons, 2nd order conformal polynomial functions have been primarily used in aerial photogrammetry during the 1960s (Baetslé 1966, Schut 1966). Due to the larger size of satellite images, they have been mainly used with georeferenced images: SPOT-HRV (level 1 and 2) using 1st order functions (Baltsavias and Stallmann 1992, Okamoto *et al.* 1998); SPOT-HRV (level 1B) and Landsat-TM (level bulk or georeferenced) using 2nd order functions (Palà and Pons 1995). More recently, 1st order affine functions were applied to IKONOS Geo products (Ahn *et al.* 2001, Fraser *et al.* 2002a, b, Jacobsen 2002, Vassilopoulou *et al.* 2002). The terms related to terrain elevation in the 3D polynomial function could be reduced to $a_iZ$ for VIR images and to $a_iZ$ and

$a_j Z^2$ for SAR images whatever the order of the polynomial functions used. The main reason is that there is no physical inter-relation in the $X$ and $Z$ or $Y$ and $Z$ directions for most of the sensors used.

In fact, Kratky (1971, 1989) already used 3rd or 4th order 3D polynomial functions with this term reduction to approximate its 2D or 3D physical models developed for ERTS or SPOT raw images respectively. The main reason for his SPOT model was that the real-time computation for implementing his specific physical model solution was not feasible on a stereo-workstation. He would certainly not do this approximation with the higher-performance computers now available. More recently, tests were also performed using Kratky's polynomial functions with IKONOS Geo products acquired with near-nadir viewing over high relief areas (Kersten *et al.* 2000, Vassilopoulou *et al.* 2002). The second study evaluated the ortho-image errors over the GCPs and 1–2 m errors were achieved depending of their number, definition and image-measurement accuracy, but this statistical evaluation is a little biased by using checked data applied in the geometric correction process. However as previously mentioned, the 3D affine transformation, also evaluated in the second study, gave the same results than 4th order polynomial functions, but with much less GCPs.

3.1.3. *3D rational functions*

While occasionally used during the 1980s (Okamoto 1981, 1988), the interest in 3D RFs has recently been renewed in the civilian photogrammetric and remote sensing communities due to the launch of the first civilian high-resolution IKONOS sensor in 1999. Since sensor and orbit parameters were not included in the meta-data, 3D RFs could be an alternative to avoid the development of 3D physical models. The 3D RFs can be used in two approaches (Madani 1999):

1. to approximate an already-solved existing 3D physical model; and
2. to normally compute the unknowns of all the polynomial functions with GCPs.

The first approach, inappropriately called terrain-independent because the process still requests DTM and some GCPs to remove RF bias (see below), is performed in two steps. A 3D regular grid of the imaged terrain is first defined and the image coordinates of the 3D grid ground points are computed using the already-solved existing 3D physical model. These grid points and their 3D ground and 2D image coordinates are then used as GCPs to resolve the 3D RFs and compute the unknown terms of polynomial functions. There are some disadvantages to RFs (Madani 1999):

- the inability to model local distortions (such as high-frequency variations with VIR sensors or with SAR sensors);
- a limitation in the image size;
- the difficulty of interpretation of the parameters due to the lack of physical meaning;
- a potential failure to zero denominator; and
- a potential correlation between the terms of polynomial functions.

A different strategy can be adopted to reduce these limitations. To improve the ability to model local distortions, RFs should be applied to georeferenced data with systematic distortions corrected (such as IKONOS Geo images) rather than raw

data with no geometric distortions corrected (such as QuickBird-2 or EROS-A1). To reduce limitation of image size, the image could be divided into sub-images, so that separate 3D RFs are required for each sub-image (Yang 2001). This results in more geometric but also radiometric processing. To prevent potential failure and correlation, the non-significant and/or high-correlated terms can be eliminated to avoid zero crossing and instability of RFs depending of image geometry (Dowman and Dolloff 2000), as mentioned previously. To overcome some of these problems, a 'universal real-time image geometry model' based on RFs has been developed (OGC 1999). This is a dynamic RF of variable orders, whose terms can be chosen as a function of the sensor geometry, and in which the denominator polynomials can be, and are generally, omitted. This reduction of terms is then similar to the orientation theory developed in the 1980s (Okamoto 1981, 1988). In addition, when the denominator polynomials are omitted, RFs become simple 3D polynomial functions, also used since the 1960s.

Dowman and Dolloff (2000) addressed the advantages of this 'universal real-time image geometry model', such as universality, confidentiality, efficiency and information transfer; and the disadvantages, such as loss of accuracy (it is not a rigorous method—this may lead to errors), numerical instability of the solution (due to over-parametrization, correlation, interpolation errors), failure for highly distorted imagery (i.e. airborne or asynchrone-mode images), uncertainty (there is no relation to physical perturbations) and complexity (in defining the functions and the number of GCPs). Some of these advantages/disadvantages are also related to 3D polynomial functions, as mentioned previously.

Image vendors and government agencies that do not want to deliver satellite/sensor information with the image and commercial photogrammetric workstation suppliers are the main users of this first approach. Image vendors thus provide with the image all the parameters of 3D RFs. Consequently, the user can directly process images without GCP for generating ortho-images with DEM, and even post-process to improve the RF parameters with GCPs. This approach was adopted by two resellers providing RF parameters with high-resolution images: Space Imaging with IKONOS Geo images (Grodecki 2001) and MacDonald, Dettwiler and Associates (MDA) with QuickBird-2 images (Hargreaves and Roberston 2001) using 3$^{rd}$ order RF parameters. Since biases or errors still exist after applying the RFs, the results need to be post-processed with few precise GCPs (at least one) (Fraser *et al.* 2002a) or the original RFs parameters can be refined with linear equations requesting more precise GCPs (Lee *et al.* 2002). The use of GCPs in post-processing and DEM in ortho-rectification is the reason why this approach is inappropriately called terrain-independent.

This first approach has also been tested under specific circumstances from an academic point of view with aerial photographs and SPOT images by computing parameters of 1$^{st}$ to 3$^{rd}$ order RFs from already-solved 3D physical models (Tao and Hu 2001) and with IKONOS Geo images by using the provided 3$^{rd}$ order RF parameters (Fraser *et al.* 2002a, b, Tao and Hu, 2002).

The second approach, called terrain-dependent, can be performed by the end-users with the same processing method as with polynomial functions. Since there are 40 and 80 parameters for the four 2$^{nd}$ and 3$^{rd}$ order polynomial functions, a minimum of 20 and 40 GCPs, respectively, are required to resolve the 3D RFs. However, the RFs do not model the physical reality of the image acquisition geometry and they are sensitive to input errors, such as the 2D/3D polynomial functions. Since RFs, such as the 2D/3D polynomial functions, mainly correct

locally at GCP locations and the distortions between GCPs are not entirely eliminated (Petrie 2002), many more GCPs will be required to reduce their error propagation in an operational environment. A piecewise approach as described previously (Yang 2001) should also be used for large images (SPOT, Landsat, IRS, RADARSAT), which will increase the number of GCPs proportionally to the number of sub-images, making the method inadequate in operational environment.

However, some academic studies in a well-controlled research environment have demonstrated the feasibility of this second approach with medium-to-high resolution images: level-1B SPOT and/or Landsat-TM georeferenced images (Okamoto *et al.* 1998, Tao and Hu 2001), RADARSAT-SAR fine mode ground range image (Dowmann and Dolloff 2000), and IKONOS Geo images (Fraser *et al.* 2002a, b, Tao and Hu 2002). Generally, the results are presented with images acquired over a flat terrain, but never over hilly or high relief areas. In fact, the solution is highly dependent on the actual terrain relief, and on the number, accuracy and distribution of GCPs (Tao and Hu 2002). For SPOT images, they found that RFs were sensitive to GCP distribution. For IKONOS images, the results were also sensitive to GCP distribution, but were not significantly better than using 3D 1$^{st}$ order polynomial functions, whereas many more GCPs are used. In fact, since the map-oriented images, such as IKONOS Geo images, are already corrected for all geometric distortions except relief, translation-rotation-scaling corrections in addition to relief correction are theoretically enough to achieve good results, such as in Fraser *et al.* (2002a, b) and Vassilopoulou *et al.* (2002). However, some of these studies and results cannot be interpreted well because the conditions of experimentation are not properly and completely defined: such as the geometric characteristics of images used, the level of geometric correction already applied to images; the source, accuracy, distribution and number of GCPs; the source, accuracy, distribution and number of checked data; the size of the terrain and its relief, etc. Consequently, their extrapolation or adaptation to other experiments should be carefully applied.

On the other hand, more recent studies using 3D RFs with different high-resolution images (level-1A EROS-A1, IKONOS Geo, level-1A QuickBird-2) showed inferior and less consistent results (Toutin *et al.* 2002, Kristóf *et al.* 2002). Some inconsistencies and errors with the IKONOS ortho-images generated from RFs were not explained (Davis and Wang 2001) while these errors did not appear using the 3D physical model. Tao and Hu (2002) achieved 2.2-m horizontal accuracy with almost 7-m bias while processing stereo IKONOS images using 1$^{st}$-approach RF method. Kristóf *et al.* (2002) and Kim and Muller (2002) obtained 5 m random errors computed on precise independent check points (ICPs) when using, respectively, precise GCPs to compute the RFs, or the RFs provided with the stereo-images and a post-processing with GCPs to remove the bias. Larger errors away from the GCPs were also reported (Petrie 2002). Since the academic results are not entirely confirmed by the end-user results, more research should be thus performed to evaluate the true applicability and the limitations of these 3D RFs for high-resolution images in an operational environment and also in any study site, especially with high relief.

### 3.2. *2D/3D physical models*

2D/3D physical functions used to perform the geometric correction differ, depending on the sensor, the platform and its image acquisition geometry:

- instantaneous acquisition systems, such as photogrammetric cameras, Metric Camera (MC) or Large Format Camera (LFC);
- rotating or oscillating scanning mirrors, such as Landsat-MSS, TM or ETM$^+$;
- push-broom scanners, such as SPOT-HRV, IRS-1C/D, IKONOS or Quickbird; and
- SAR sensors, such as JERS, ERS-1/2, RADARSAT-1/2 or ENVISAT.

Although each sensor has its own unique characteristics, one can draw generalities for the development of 2D/3D physical models, in order to fully correct all distortions described previously. The physical model should mathematically model all distortions of the platform (position, velocity, attitude for VIR sensors), the sensor (viewing angles, panoramic effect), the Earth (ellipsoid and relief for 3D) and the cartographic projection. The geometric correction process can address each distortion one by one and step by step or simultaneously. In fact, it is better to consider the total geometry of viewing (platform + sensor + Earth + map), because some of their distortions are correlated and have the same type of impact on the ground. It is theoretically more precise to compute one 'combined' parameter only than each component of this 'combined' parameter, separately, avoiding also over-parameterization and correlation between terms.

Some examples of 'combined' parameters include:

- the 'orientation' of the image is a combination of the platform heading due to orbital inclination, the yaw of the platform and the convergence of the meridian;
- the 'scale factor' in the along-track direction is a combination of the velocity, the altitude and pitch of the platform, the detection signal time of the sensor and the component of the Earth rotation in the along-track direction; and
- the 'levelling angle' in the across-track direction is a combination of platform roll, viewing angle, orientation of the sensor and Earth curvature; etc.

Considerable research has been carried out in the development of robust and rigorous 3D physical models describing the acquisition geometry related to different types of images (VIR and SAR, low, medium and high resolution) and of platforms (spaceborne and airborne). 2D physical model was developed for ERTS imagery (Kratky 1971) and 3D physical models were developed:

- for low/medium-resolution VIR satellite images (Bähr 1976, Masson d'Autume 1979, Sawada *et al.* 1981, Khizhnichenko 1982, Friedmann *et al.* 1983, Guichard 1983, Toutin 1983, Salamonowicz 1986, Gugan 1987, Konecny *et al.* 1986, 1987, Kratky 1987, Shu 1987, Paderes *et al.* 1989, Westin 1990, Robertson *et al.* 1992, Ackermann *et al.* 1995, Sylvander *et al.* 2000, Westin 2000);
- for high-resolution VIR satelitte images (Gopala Krishna *et al.* 1996, Jacobsen 1997, Cheng and Toutin 1998, Toutin and Cheng 2000, 2002, Bouillon *et al.* 2002, Chen and Teo 2002, Hargreaves and Roberston 2001, Toutin 2003a, Westin and Forsgren 2002);
- for SAR satellite images (Rosenfield 1968, Gracie *et al.* 1970, Leberl 1978, Wong *et al.* 1981, Curlander 1982, Naraghi *et al.* 1983, Guindon and Adair 1992, Toutin and Carbonneau 1992, Tannous and Pikeroen 1994);
- for VIR airborne images (Derenyi and Konecny 1966, Konecny 1976, Gibson 1984, Ebner and Muller 1986, Hofmann and Muller 1988); and

- for airborne SLAR/SAR images (LaPrade 1963, Rosenfield 1968, Gracie *et al.* 1970, Derenyi 1970, Konecny 1970, Leberl 1972, Hoogeboom *et al.* 1984, Toutin *et al.* 1992) and many others afterwards.

The 2D Kratky's physical model for ERTS took into consideration and mathematically modelled, step-by-step, the effects of scanner geometry, panoramic effect, earth rotation, satellite circular orbit and attitude, non-uniform scan rate and map projection to finalize with a dual simple equation (one for each axis), which mathematically integrated all the previous error equations.

The general starting points of the other research studies to derive the mathematical functions of the 3D physical model are generally:

1. the well-known collinearity condition and equations (Bonneval 1972, Wong 1980) for VIR images:

$$x = (-f)\frac{m_{11}(X-X_0)+m_{12}(Y-Y_0)+m_{13}(Z-Z_0)}{m_{31}(X-X_0)+m_{32}(Y-Y_0)+\mathrm{m}_{33}(Z-Z_0)} \tag{4}$$

$$y = (-f)\frac{m_{21}(X-X_0)+m_{22}(Y-Y_0)+m_{23}(Z-Z_0)}{m_{31}(X-X_0)+m_{32}(Y-Y_0)+m_{33}(Z-Z_0)} \tag{5}$$

   where: $(x,y)$ are the image coordinates; $(XYZ)$ are the map coordinates; $(X_0\,Y_0Z_0)$ are the projection centre coordinates; $-f$ is the focal length of the VIR sensor; and $[m_{ij}]$ are the nine elements of the orthogonal 3-rotation matrix.
2. The Doppler and range equations for radar images:

$$f = \frac{2(\overrightarrow{V_S}-\overrightarrow{V_P})(\overrightarrow{S}-\overrightarrow{P})}{\left|\overrightarrow{S}-\overrightarrow{P}\right|}, \tag{6}$$

$$r = \left|\overrightarrow{S}-\overrightarrow{P}\right|, \tag{7}$$

   where: $f$ is the Doppler value; $r$ is the range distance; $\overrightarrow{S}$ and $\overrightarrow{V_S}$ are the sensor position and velocity; $\overrightarrow{P}$ and $\overrightarrow{V_P}$ are the target point position and velocity on the ground; and $\lambda$ is the radar wavelength.

It should be noted that the collinearity equations were adapted as radargrammetric equations to process radar images (Leberl 1972, 1990) and later as an integrated and unified mathematic equations to process multi-sensor (VIR or radar) images (Toutin 1995b).

The collinearity equations are valid for an instantaneous image or scanline acquisition, such as photogrammetric cameras (LFC, MC), VIR scanner sensors (SPOT, Landsat) and the Doppler-range equations are valid for a SAR scanline. However, since the parameters of neighbouring scanlines of scanners are highly correlated, it is possible to link the exposure centres and rotation angles of the different scanlines to integrate supplemental information, such as:

- the ephemeris and attitude data using celestial mechanic laws (figure 2) for satellite images; or
- the global positioning system (GPS) and inertial navigation system (INS) data for airborne images.

The integration of the different distortions and the mathematical derivation of equations for different sensors are outside the scope of this paper. They are

described for photogrammetric cameras in Bonneval (1972) and Wong (1980), for scanner images in Leberl (1972), Konecny (1976) and Masson d'Autume (1979), for ERTS/Landsat images in Kratky (1971), Bähr (1976) and Salamonowicz (1986), for push-broom scanners, such as SPOT, in Guichard (1983), Toutin (1983) and Konecny *et al.* (1986, 1987), and for SAR data in Leberl (1978) and Curlander (1982).

## 4. Methods, processing and errors

Whatever the mathematical functions used, the geometric correction method and processing steps are more or less the same. The processing steps are (figure 3):

- acquisition of image(s) and *pre-processing of metadata*;
- acquisition of the ground points (control/check/pass) with image coordinates and map coordinates $X$, $Y$, **($Z$)**;
- computation of the unknown parameters of the mathematical functions used for the geometric correction model for one or more images; and
- image(s) rectification **with or** without DEM.

The main differences in the processing steps between physical and empirical models are in *italic style* and between 2D and 3D models are in **bold style**. The metadata are useless for empirical models because the models do not reflect the geometry of viewing, while the $Z$-elevation coordinates for GCPs and DEM are of no use for 2D empirical models.

### 4.1. *Acquisition of images and metadata*

With VIR images, different types of image data with different levels of pre-processing can be obtained, but the different image providers unfortunately use a

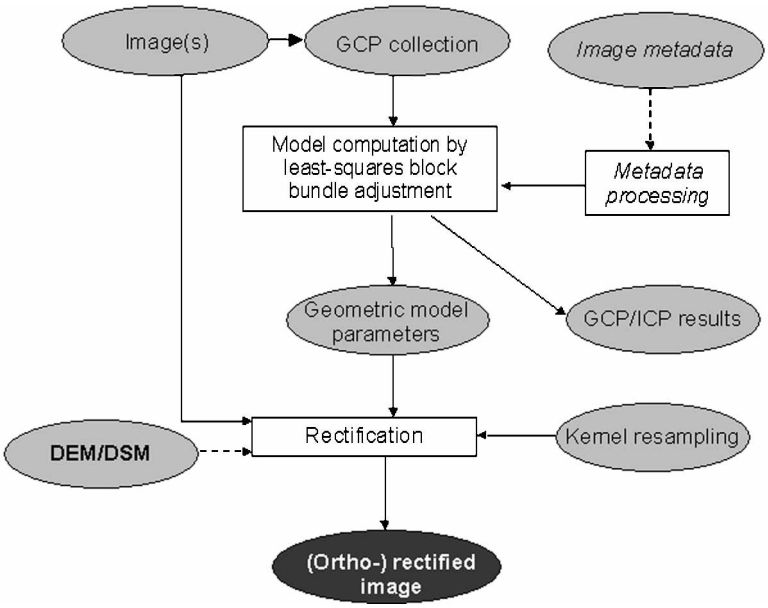


Figure 3. Description of the geometric correction method and processing steps. The ellipse symbols are input/output data and the box symbols are processes.

range of terminology to denominate the same type of image data. Standardization should be better defined, mainly for the convenience of end-users:

- raw images with only normalization and calibration of the detectors (e.g. level 1A for SPOT and basic for EROS-A1 or QuickBird-2) without any geometric correction are satellite-track oriented. In addition, full metadata related to sensor, satellite (ephemeris and attitude) and image are provided;
- geo-referenced images (e.g. level 1B for SPOT or 1G for Landsat-ETM$^+$) corrected for systematic distortions due to the sensor, the platform and the Earth rotation and curvature are satellite-track oriented. Generally, few metadata related to sensor and satellite are provided; some of metadata are related to the 1B processing; or
- map-oriented images, also called geocoded images, (e.g. level 2A for SPOT, Cartera Geo for IKONOS or Standard for QuickBird-2) corrected for the same distortions as geo-referenced images are North oriented. Generally, very few metadata related to sensor and satellite are provided; most of metadata are related to the 2A processing and the ellipsoid/map characteristics.

For simplicity, the easiest terminology defined for SPOT images are used. The raw 'level 1A' images are preferred by photogrammetrists because 3D physical models derived from co-linearity equations are well known and developed and easily used in softcopy workstations. Since different 3D physical models are largely available for such VIR images, raw 1A-type images should be now favoured by the remote sensing community too. Specific software to read and pre-process the appropriate metadata (ephemeris, attitude, sensor and image characteristics) have to be realized for each image sensor according to the 3D physical model used. Using celestial mechanics laws and Lagrange equations (Escobal 1965, Centre National d'Études Spatiales 1980, Light *et al.* 1980) the ephemeris (position and velocity) can be transformed into specific osculatory orbital parameters to reduce the time-related effects (figure 2) (Toutin 1983). Since the Lagrange equations take into account the variation of the Earth gravitational potential to link the different positions of the satellite during the image formation, it is more accurate and robust than using a constant ellipse with 2$^{nd}$ order time-dependent polynomial functions (Guichard 1983, Toutin 1983, Tannous and Pikeroen 1994, Bannari *et al.* 1995). This statement is more applicable when 'long-strip' images from a same orbit are used with low-resolution images (Robertson *et al.* 1992, Sylvander *et al.* 2000, Westin 2000), with images path processing (Toutin 1985, Sakaino *et al.* 2000) or a block bundle adjustment method (Veillet 1991, Campagne 2000, Kornus *et al.* 2000, Cantou 2002, Toutin 2002b, c, 2003). 3D physical models were also applied to high-resolution airborne images (Konecny 1976, Gibson 1984, Ebner and Muller 1986) or spaceborne images, such as IRS–1C/D (Gopala Krishna *et al.* 1996, Jacobsen 1997, Cheng and Toutin 1998), EROS (Chen and Teo 2002, Westin and Forsgren 2002), SPOT-5 (Bouillon *et al.* 2002) and QuickBirb-2 (Hargreaves and Roberston 2001, Toutin and Cheng 2002) for achieving pixel accuracy or better. Some results were presented using 3D RFs with SPOT images (Dowman and Dolloff 2000, Tao and Hu 2001), but the conditions of experimentation (study site and terrain relief, image characteristics, cartographic data and accuracy, polynomial order) were not fully explained. To our knowledge, no results were published with high-resolution airborne or spaceborne images (EROS-A1, SPOT-5, QuickBird-2) using 3D RF's due their inability to model high-frequency distortions inherent to raw level-1A images (Madani 1999, Dowman and Dolloff 2000).

Since they have been systematically corrected and georeferenced, the 'level 1B' images just retain the terrain elevation distortion, in addition to a rotation-translation related to the map reference system. A 3D 1st order polynomial model with *Z*-elevation parameters could thus be efficient depending of the requested final accuracy. For scanners with across-track viewing capability, only the *Z*-elevation parameter in the *X*-equation is useful. The 2nd order polynomial models could also be used (Palà and Pons 1995) for correcting some residual errors of the 1B processing. When possible, solutions to overcome the empirical model approximation are either to convert the 1B-images back into 1A-images using the metadata and the reverse transformation (Al-Roussan *et al.* 1997), or to 're-shape and re-size' the 1B-images to the raw imagery format (Valadan Zoej and Petrie 1998). This 1B-geometric modelling can be mathematically combined with normal level-1A 3D physical model to avoid multiple image resampling. Although this mathematical procedure used for 1B images works better than empirical models, it is still recommended that raw images with 3D rigorous physical models (co-linearity equations) be directly used.

The map-oriented images ('level 2A') also retain the elevation distortion but image lines and columns are no more related to sensor-viewing and satellite directions. A 3D 1st order polynomial model with Z-elevation parameters in both axes can thus be efficient depending of the requested final accuracy. Such as for level 1B, 2nd order empirical models (polynomial or rational) can be used for correcting some residual errors of the 2A processing, but it is generally no longer possible to convert back the 2A image with the reverse transformation. Due to the fact that IKONOS Geo images are already corrected for the systematic geometric distortions, 2D/3D empirical models were recently applied to achieve pixel accuracy or better:

- 2D first-order polynomial and RF functions (Hanley and Fraser 2001);
- 3D first-order polynomial functions (Ahn *et al.* 2001, Fraser *et al.* 2002a,b, Vassilopoulou *et al.* 2002);
- 3D fourth-order polynomial functions (Kersten *et al.* 2000, Vassilopoulou *et al.* 2002);
- 3D third-order RF functions using the 1st approach (described in §3.1.3) with parameters computed from the Space Imaging camera model (Grodecki 2001, Fraser *et al.* 2002a,b, Tao and Hu 2002); and
- 3D third-order RF functions using the 1st approach (described in §3.1.3) with parameters provided with Geo images and using GCPs either to remove bias (Fraser *et al.* 2002a) or to improve the original RF parameters (Lee *et al.* 2002).

Although the results are in the order of pixel accuracy or sometimes better, and are correlated with GCP definition and image-measurement accuracy, they were generally achieved using images or sub-images acquired over flat terrain and processed with very accurate cartographic data (0.10 m). Only few results were published in high relief terrain using 3D polynomial functions (Kersten *et al.* 2000, Vassilopoulou *et al.* 2002). However, they were all achieved in an academic environment or by the image providers where errors and processing are well controlled. Since other academic or operational studies using the 1st or 2nd RF approach obtained larger errors of few (2–5) pixels (Davis and Wang 2001, Kristóf *et al.* 2002, Kim and Muller 2002, Petrie 2002, Tao and Hu 2002 and other unpublished studies), care must be then taken by end-users in the extrapolation of these results using empirical models in operational environments to any

high-resolution image acquired over any terrain and processed with any cartographic data.

However, a 3D physical model has been approximated and developed for IKONOS Geo images using basic information of the metadata and celestial mechanics laws (Toutin and Cheng 2000). Even approximated, this 3D physical model ('using a global geometry and adjustment') has been proven to be robust and to achieve consistent results over different study sites and environments (urban, semi-rural, rural, Europe, North and South America), different relief (flat to high) and different cartographic data (DGPS, ortho-photos, digital topographic maps, DEM) (Toutin 2003a). This 3D physical model has been used in different applications, such as for digital image basemap generation (Davis and Wang 2001), in urban management (Hoffman *et al.* 2001, McCarthy *et al.* 2001, Meinel and Reder 2001, Ganas *et al.* 2002) or in land resources management (Kristóf *et al.* 2002, Toutin 2003b).

SAR images are standard products in slant or ground range presentations. They are generated digitally during post-processing from the raw signal SAR data (Doppler frequency, time delay). Errors present in the input parameters related to image geometry model will propagate through to the image data. These include errors in the estimation of slant range and of Doppler frequency and also errors related to the satellite's ephemeris and the ellipsoid. Assuming the presence of some geometric error residuals, the parameters of a 3D physical model reflect these residuals. As mentioned previously, the 3D physical model starts generally either from the traditional Doppler and range equations (Curlander 1982), from the equations of radargrammetry (Konecny 1970, Leberl 1978, 1990), or from generalized equations (Leberl 1972, Masson d'Autume 1979, Toutin 1995b). Due to the large elevation distortions in SAR images, 2D polynomial models cannot be used, even in rolling topography (Toutin 1995a) or to extract planimetric features (de Sève *et al.* 1996). Furthermore, since different 3D SAR physical models are largely available, few attempts have been done to apply 3D polynomial or RF empirical models to SAR images (spaceborne or airborne). Dowman and Dolloff (2000) presented preliminary results with one RADARSAT-1 SAR fine mode image but the conditions of experimentation (study site and terrain relief, cartographic data and accuracy, type and approach of RFs) were not described. Extrapolation to other SAR data is not therefore recommended.

### 4.2. *Acquisition of GCPs*

Whatever the VIR and/or SAR geometric model used, even with the RF 'terrain-independent' approach to remove the bias or refine RF parameters, some GCPs have to be acquired to compute/refine the parameters of the mathematical functions in order to obtain a cartographic standard accuracy. Generally, an iterative least-square adjustment process is applied when more GCPs than the minimum number required by the model (as a function of unknown parameters) are used. The number of GCPs is a function of different conditions: the method of collection, sensor type and resolution, image spacing, geometric model, study site, physical environment, GCP definition and accuracy and the final expected accuracy. If GCPs are determined *a priori* without any knowledge of the images to be processed 50% of the points may be rejected. If GCPs are determined *a posteriori* with knowledge of the images to be processed, the reject factor will be smaller (20–30%). Consequently, all the aspects of GCP collection do not have to be

considered separately, but as a whole to avoid too large discrepancies in accuracy of these different aspects. For example, differential GPS survey should not be used to process Landsat data in mountainous study site, nor should road intersections and 1 : 50 000 topographic maps be used to process QuickBird images if 1–2 m final accuracy is expected, etc. The weakest aspect in GCP collection, which is of course different for each study site and image, will thus be the major source of error in the error propagation and overall error budget of the bundle adjustment.

Since empirical models do not reflect the geometry of viewing and do not filter errors, many more GCPs than the theoretical minimum are required to reduce the propagation of input errors in the geometric models. When the cartographic data accuracy and/or the positioning accuracy are in the same order of magnitude as the image resolution, twice as many is a minimum requirement: around 20, 40 or 80 GCPs should then be acquired for 2nd order 2D polynomial, 3D polynomial or 3D terrain-dependent RF models respectively. The 3rd order models obviously required more GCPs, mainly RFs. Furthermore, to insure robustness and consistency in an operational environment, it is safer to collect more than twice the minimum required mentioned previously. This could therefore be a restriction in the use of such empirical models in an operational environment. However, when using 3D 1st-approach RF models with the already-computed parameters provided by the image vendor, a few (1–10) GCPs only are needed to remove the bias or to refine the RF parameters. When more than one image is processed, each image requires its own GCPs and the geometric models are generally computed separately (no relative orientation or link between adjacent images). However, some block adjustment can be performed with RFs (Dial and Grodecki 2002, Fraser *et al.* 2002a). Since empirical models are sensitive to GCP distribution and number, GCPs should be spread over the full image(s) in planimetry and also in the elevation range for the 3D models to avoid large errors between GCPs. It is also better to have medium-accurate GCPs (lakes, tracks, ridges) than no GCP at the tops of mountains. If the image is larger than the study site it is recommended to reduce the GCP collection to the study site area because the empirical models only correct locally.

With 3D physical models, fewer GCPs (1–6) are theoretically required per image. When more than one image is processed a spatio-triangulation method with 3D block-bundle adjustment can be used to process all images together (VIR and SAR). It enables users to reduce drastically the number of GCPs for the block with the use of tie points (TPs) (Veillet 1991, Belgued *et al.* 2000, Campagne 2000, Kornus *et al.* 2000, Sakaino *et al.* 2000, Cantou 2002, Toutin 2003b, c, d). When the map and positioning accuracy is of the same order of magnitude as the image resolution, twice (or a little less) the theoretical minimum is recommended. When the accuracy is worse, the number should be increased depending also on the final expected accuracy (Savopol *et al.* 1994). Since more confidence, consistency and robustness can be expected with physical models (global image processing, filtering input errors) than with empirical models, it is not necessary to increase the number of GCPs in operational environments. GCPs should preferably be spread at the border of the image(s) to avoid extrapolation in planimetry, and it is also preferable to cover the full elevation range of the terrain (lowest and highest elevations). Contrary to empirical models, it is not necessary to have a regular distribution in the planimetric and elevation ranges. Since the physical models correct globally the GCP collection has to be performed in the full image size, even if the study site is smaller. First, it will be easier to find GCPs over the full image

than over a sub-area and more homogeneity is thus obtained in the different area of the image.

GCP cartographic co-ordinates can be obtained from global positioning system (GPS), air photo surveys, paper or digital maps, GIS, ortho-rectified photos or images, chip database, etc, depending on the requested accuracy of the input/output data. The cartographic co-ordinates obtained from these sources have drastically different accuracies: from better than 0.2 m with differential GPS to 25–50 m with 1 : 50 000 paper maps, certainly the most common GCP source used around the world. Consequently, with lower accuracy more GCPs must be used (Savopol *et al.* 1994). The image co-ordinates are obtained interactively on the screen or automatically using GCP chip database and image correlation tools. When more than multiple images with overlapping coverage are processed the image co-ordinates are obtained either in stereoscopy (the best solution) or simultaneously in 'double monoscopy' because some workstations do not have full stereoscopic capabilities for multi-sensor images. The 'double monoscopy' image measurements will then create artificial *X*- and *Y*-parallaxes (a few pixels) between the images, and the parallax errors will propagate through the bundle adjustment (relative and absolute orientations). The error propagation is larger with SAR images than with VIR images due to a lower image-measurement accuracy (1–2 pixels versus ⅓–½ pixel), and increases with smaller intersection angles, but also with shallower same-side SAR look angles (Toutin 1998, 1999). Consequently, where possible, true stereoscopic image measurements with human depth perception should be used. These enable a better relative correspondence of the GCP between the images and a better absolute positioning on the ground.

### 4.3. *Geometric model computation*

When more than one image (VIR or SAR) is processed over a large study site (figure 4), a spatio-triangulation process based on a block adjustment can be first applied simultaneously to compute all geometric models (figure 3). The spatio-triangulation method has been developed and applied with different VIR/SAR/HR data using 3D physical models (Veillet 1991, Belgued *et al.* 2000, Campagne 2000, Kornus *et al.* 2000, Sakaino *et al.* 2000, Cantou 2002, Toutin 2003b, c, d), as well as with IKONOS data using 3D RF models (Dial and Grodecki 2002, Fraser *et al.* 2002). The first group of tests was achieved over different terrain including mountainous areas while the last group of tests was only achieved over flat terrain. Figure 4 is an example of a block over the Canadian Rocky Mountains (BC) (600 km by 530 km) with 15 level-1G Landsat-ETM$^+$ images formed with five strips and three rows (Toutin 2003c).

All model parameters of each image/strip are determined by a common least-squares adjustment so that the individual models are properly tied in and the entire block is optimally oriented in relation to the GCPs. With the spatio-triangulation process, the same number of GCPs is theoretically needed to adjust a single image, an image strip or a block. However, some tie points (TPs) between the adjacent images have to be used to link the images and/or strips. Elevation of TPs (ETPs) must be added when the intersection geometry of the adjacent images is weak, such as with intersection angles less than 15°–20° (Toutin 2003b, c, d). There are a number of advantages to the spatio-triangulation process, namely:

- the reduction of the number of GCPs;
- a better relative accuracy between the images can be obtained;

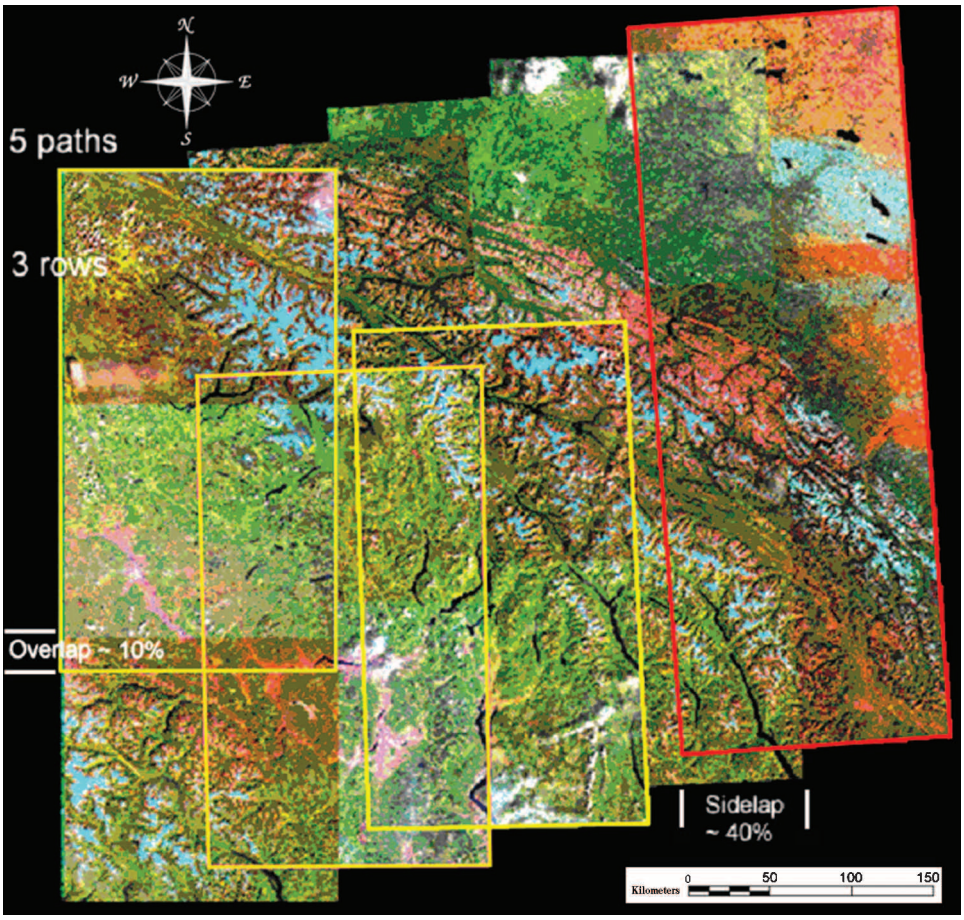


Figure 4. Image block of 15 level-1G Landsat-7 ETM$^+$ images over Rocky Mountains, Canada (600 km × 530 km) generated from five strips and three rows. The lined images are acquired from the same orbit and date and can be used as a single image with path processing (Toutin 2003c).

- a more homogeneous and precise mosaic over large areas can be obtained; and
- a homogeneous GCP network can be generated for future geometric processing.

Whatever the number of images (spatio-triangulation or single image) and the geometric models (physical or empirical) used, each GCP contributes to two observation equations: an equation in $X$ and an equation in $Y$. The observation equations are used to establish the error equations for GCPs, TPs, and ETPs. Each group of error equations can be weighted as a function of the accuracy of the image and cartographic data. The normal equations are then derived and resolved with the unknowns computed. In addition for the 3D physical models, conditions or constraints on osculatory orbital parameters or other parameters (GPS/INS) can be added in the adjustment to take into account the knowledge and the accuracy of the ephemeris or other data, when available. They thus prevent the adjustment from diverging and they also filter the input errors.

Since there are always redundant observations, in order to reduce the input error propagation in the geometric models a least-square adjustment is generally

used. When the mathematical equations are nonlinear, which is the case for physical and 2nd and higher order empirical models, some means of linearization (series expansions or Taylor's series) must be used. A set of approximate values for the unknown parameters in the equations must be thus initialized:

- to zero for the empirical models, because they do not reflect the image acquisition geometry; or
- from the osculatory orbital/flight and sensor parameters of each image for the physical models.

More information on least-squares methods applied to geomatics data can be obtained in Mikhail (1976) and Wong (1980). The results of this processing step are:

- the parameter values for the geometric model used for each image;
- the residuals in $X$ and $Y$ directions (and $Z$ if more than one image is processed) for each GCP/ETP/TP and their root mean square (rms) residuals;
- the errors and bias in $X$ and $Y$ directions (and $Z$ if more than one image is processed) for each ICP if any, and their rms errors; and
- the computed cartographic coordinates for each point, including ETPs and TPs.

When more GCPs than the minimum theoretically required are used, the GCP rms residuals reflect the modelling accuracy, while the ICP rms errors reflect the final accuracy taking into account ICP accuracy. As mentioned previously, this final accuracy is mainly dependent on the geometric model and the number of GCPs used versus their cartographic and image co-ordinate errors. When ICPs are not accurate, their errors are included in the computed rms errors; consequently, the final internal accuracy of the modelling will be better than these rms errors.

When no ICP is available, GCP rms residuals can be carefully used as an approximation of the final accuracy, only when using physical models. However, the fact that GCP rms residuals can be small with empirical models does not indicate necessarily a good accuracy because these models correct locally at GCPs and the least-square adjustment minimizes residuals at GCPs. Errors are still present between GCPs (Davies and Wang 2001, Petrie 2002). On the other hand by using overabundant GCPs with physical models, the input data errors (image measurement and/or map) do not propagate through the physical models but are mainly reflected in the GCP residuals due to a global adjustment. Consequently, it is thus 'normal and safe' with 3D physical models to obtain RMS residuals in the same order of magnitude than the GCP accuracy, but the physical model by itself will be more accurate: in other words, the internal accuracy of image(s) will be better than the rms residuals. In contrast to empirical methods, which are sensitive to GCP number and spatial distribution (including their elevation), the 3D physical models are not affected by these factors because they precisely retain the complete viewing geometry, provided that there is no extrapolation in planimetry and also in elevation.

### 4.4. *Image rectification*

The last step of the geometric processing is image rectification (figure 3). To rectify the original image into a map image, there are two processing operations:

- a geometric operation to compute the cell coordinates in the original image for each map image cell; and

- a radiometric operation to compute the intensity value or digital number (DN) of the map image cell as a function of the intensity values of original image cells that surround the previously-computed position of the map image cell.

4.4.1. *Geometric operation*

The geometric operation requires the two equations of the geometric model with the previously computed unknowns, and sometimes elevation information. Since 2D models do not use elevation information, the accuracy of the resulting rectified image will depend on the image viewing/look angle and the terrain relief. On the other hand, as 3D models take into account elevation distortion DEM is thus needed to create precise ortho-rectified images. This rectification should then be called an ortho-rectification. But if no DEM is available, different altitude levels can be input for different parts of the image (a kind of 'rough' DEM) to minimize this elevation distortion. It is then important to have a quantitative evaluation of the DEM impact on the rectification/ortho-rectification process, both in terms of elevation accuracy for the positioning accuracy and of grid spacing for the level of details. This last aspect is more important with high-resolution images because a poor grid spacing when compared to the image spacing could generate artefacts for linear features (wiggly roads or edges).

Figures 5 and 6 give the relationship between the DEM accuracy (including interpolation in the grid), the viewing and look angles with the resulting positioning error on VIR and SAR ortho-images, respectively. These curves were mathematically computed with the elevation distortion parameters of a 3D physical model (Toutin 1995b). However, they could be also used as approximation for other 3D physical and empirical models. One of the advantages of these curves is that they can be used to find any third parameter when the two others are known. This can be useful not only for quantitative evaluation of the ortho-rectification,

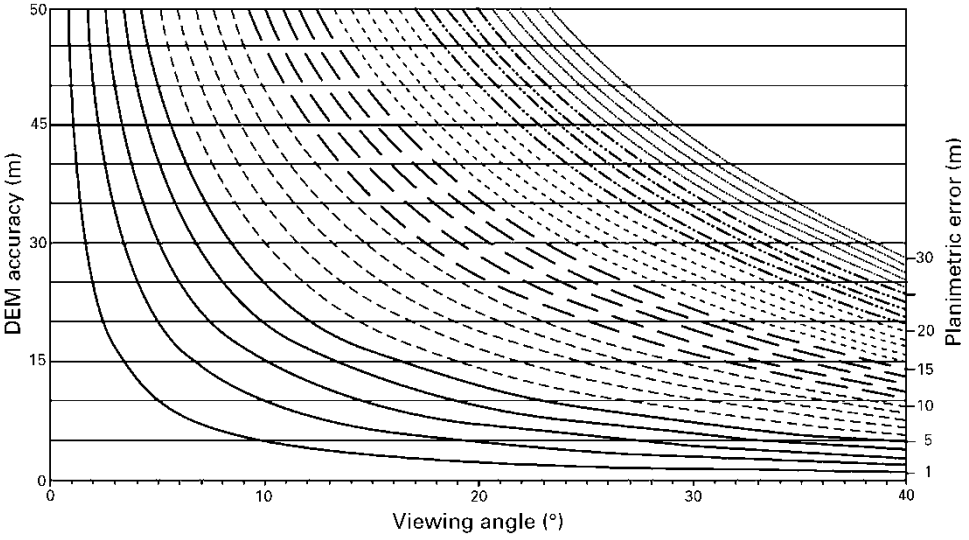


Figure 5. Relationship between the DEM accuracy (m), the viewing angle (°) of the VIR image, and the resulting positioning error (in metres) generated on the ortho-image (Toutin 1995b).

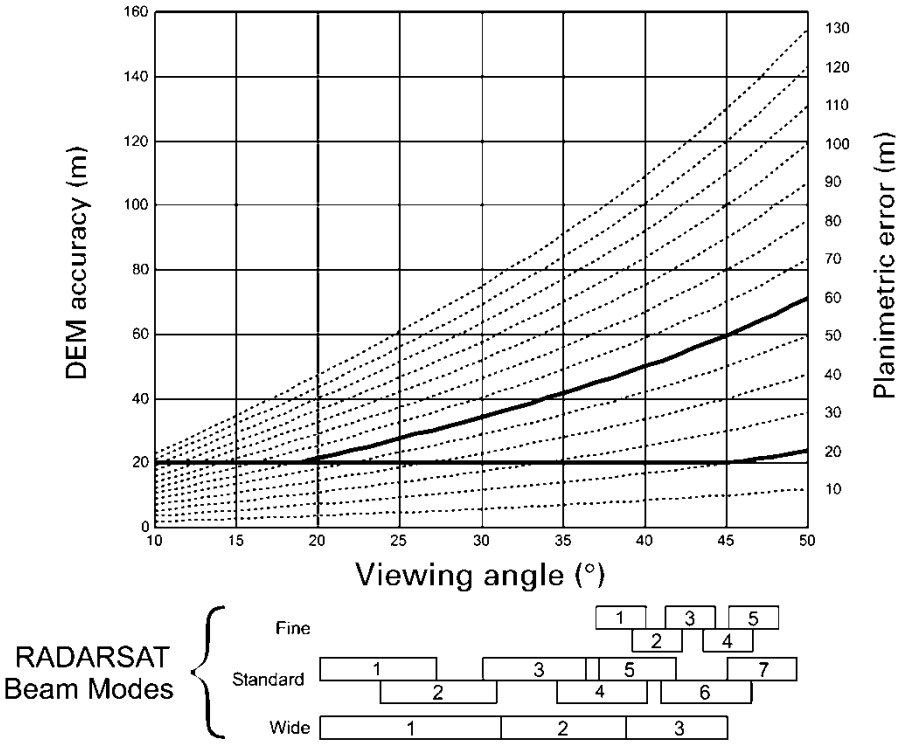


Figure 6. Relationship between the DEM accuracy (m), the look angle (°) of the SAR image, and the resulting positioning error (in metres) generated on the SAR ortho-image. The different boxes at the bottom represent the range of look angles for each RADARSAT beam mode. (Toutin 1998).

but to forecast the appropriate input data, DEM or the viewing/look angles, depending of the objectives of the project.

For example (figure 5), with a SPOT image acquired with a viewing angle of 10° and having a 45 m accurate DEM, the error generated on the ortho-image is 9 m. Inversely, if a 4 m final positioning accuracy for the ortho-image is required and having a 10-m accurate DEM, the VIR image should be acquired with a viewing angle less than 20°. The same error evaluation can be applied to SAR data using the curves of figure 6. As another example, if positioning errors of 60 m and 20 m on standard-1 (S1) and fine-5 (F5) ortho-images, respectively are required, a 20 m elevation error, which includes the DEM accuracy and the interpolation into the DEM, is thus sufficient. For high-resolution images (spaceborne or airborne), the surface heights (buildings, forest, hedges) should be either included in the DEM to generate a digital surface model (DSM) or taken into account in the overall elevation error. In addition, an inappropriate DEM in term of grid spacing can generate artifacts with high-resolution images acquired with large viewing angles, principally over high relief areas (Zhang *et al.* 2001).

Finally, for any map coordinates ($X$, $Y$), with the $Z$-elevation extracted from a DEM when 3D models are used, the original image coordinates (column and line) is computed from the two resolved equations of the model. However, the computed image coordinates of the map image coordinates will not directly overlay in the

original image; in other words, the column and line computed values will rarely, if ever, be integer values.

4.4.2. *Radiometric operation*

Since the computed coordinate values in the original image are not integers, one must compute the DN to be assigned to the map image cell. In order to do this, the radiometric operation uses a resampling kernel applied to original image cells: either the DN of the closest cell (called nearest neighbour resampling) or a specific interpolation or deconvolution algorithm using the DNs of surrounding cells. In the first case, the radiometry of the original image and the image spectral signatures are not altered, but the visual quality of the image is degraded. In addition to the radiometric degradation, a geometric error of up to half pixel is also introduced. This can cause a disjointed appearance in the map image. If these visual and geometric degradations are acceptable for the end user, it can be an advantageous solution.

In the second case, different interpolation or deconvolution algorithms (bilinear interpolation or sinusoidal function) can be applied. The bilinear interpolation takes into account the four cells surrounding the cell. The final DN is then either computed from two successive linear interpolations in line and column using DNs of the two surrounding cells in each direction or in one linear interpolation using DNs of the four surrounding cells. The DNs are weighted as a function of the cell distance from the computed coordinate values. Due to the weighting function this interpolation creates a smoothing in the final map image.

The theoretically ideal deconvolution function is the $\sin(x)/x$ function. As this function has an infinite domain it cannot be exactly computed. Instead, it can be represented by piecewise cubic function, such as the wellknown cubic convolution. The cubic convolution then computes $3^{rd}$ order polynomial functions using a $4 \times 4$ cell window. DNs are first computed successively in the four-column and -line direction, and the final DN is an arithmetical mean of these DNs. This cubic convolution does not smooth, but enhances and generates some contrast in the map image (Kalman 1985).

Due to computer improvement over recent years, the $\sin(x)/x$ function can now be directly applied as deconvolution function with different window sizes (generally $8 \times 8$ or $16 \times 16$). The computation time with $16 \times 16$ cell window can be 40–80 times more than the computation time for nearest neighbour resampling. The final image is, of course, sharper with more detailed features.

All these interpolation or deconvolution functions can be applied to VIR or SAR images. However, they are geometric resampling kernels, not very well adapted to SAR images. Instead, it is better to use statistical functions based on the characteristics of the radar, such as existing adaptive filters using local statistics (Lee 1980, Lopes *et al.* 1993, Touzi 2002). Combining filtering with resampling also avoids multiple radiometric processing and transformation, which largely degrades the image content and its interpretation (Toutin 1995b).

Since interpolation or deconvolution functions transform the DNs and then alter the radiometry of the original image, problems may be encountered in subsequent spectral signature or pattern recognition analysis. Consequently, any process based on image radiometry should be performed before using interpolation or deconvolution algorithms.

Figures 7 and 8 are examples of the application of different resampling kernels

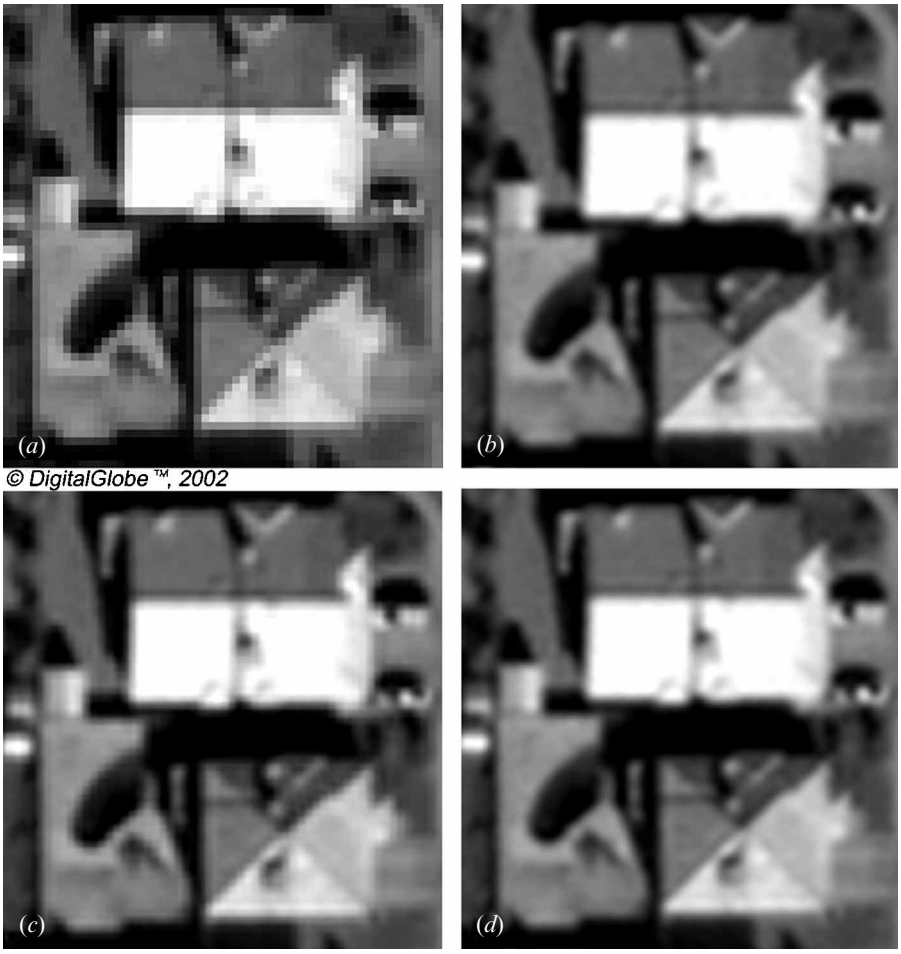


Figure 7. Examples of applications of geometric resampling kernels used in the rectification process with a Quickbird image. The sub-images are 350 by 350 pixels with 0.10-m spacing. Letters A, B, C and D refer to different geometric resampling kernels (nearest neighbour, bilinear, cubic convolution, $\sin(x)/x$ with $16 \times 16$ window), respectively. Quickbird Image © Digital Globe, 2001.

with Quickbird high-resolution VIR image and RADARSAT-SAR fine mode (F5) images, respectively. Sub-images ($200 \times 200$ pixels) were resampled with a factor of six to better illustrate the variations of the resampling kernels: the Quickbird and RADARSAT resampled image pixels are then 0.10 m and 1.10 m, respectively. The letters A, B, C and D refer to different geometric resampling kernels (nearest neighbour, bilinear, cubic convolution, $\sin(x)/x$ with $16 \times 16$ window), respectively and the letters E and F refer to statistical SAR filters (Enhanced Lee and Gamma), respectively. For both VIR and SAR images, the nearest neighbour resampling kernel (A) generates 'blocky' images with rectangular-edge features, while the bilinear resampling kernel (B) generates fuzzy images with the feeling of 'out of focus' images. The best results are obtained with the sinusoidal resampling kernels (C and D): even if there are few differences the true sinusoidal function (D) generates sharper features. As an example on the Quickbird image (figure 7), the two cars in the front of the houses are better defined in D: the windshield and rear

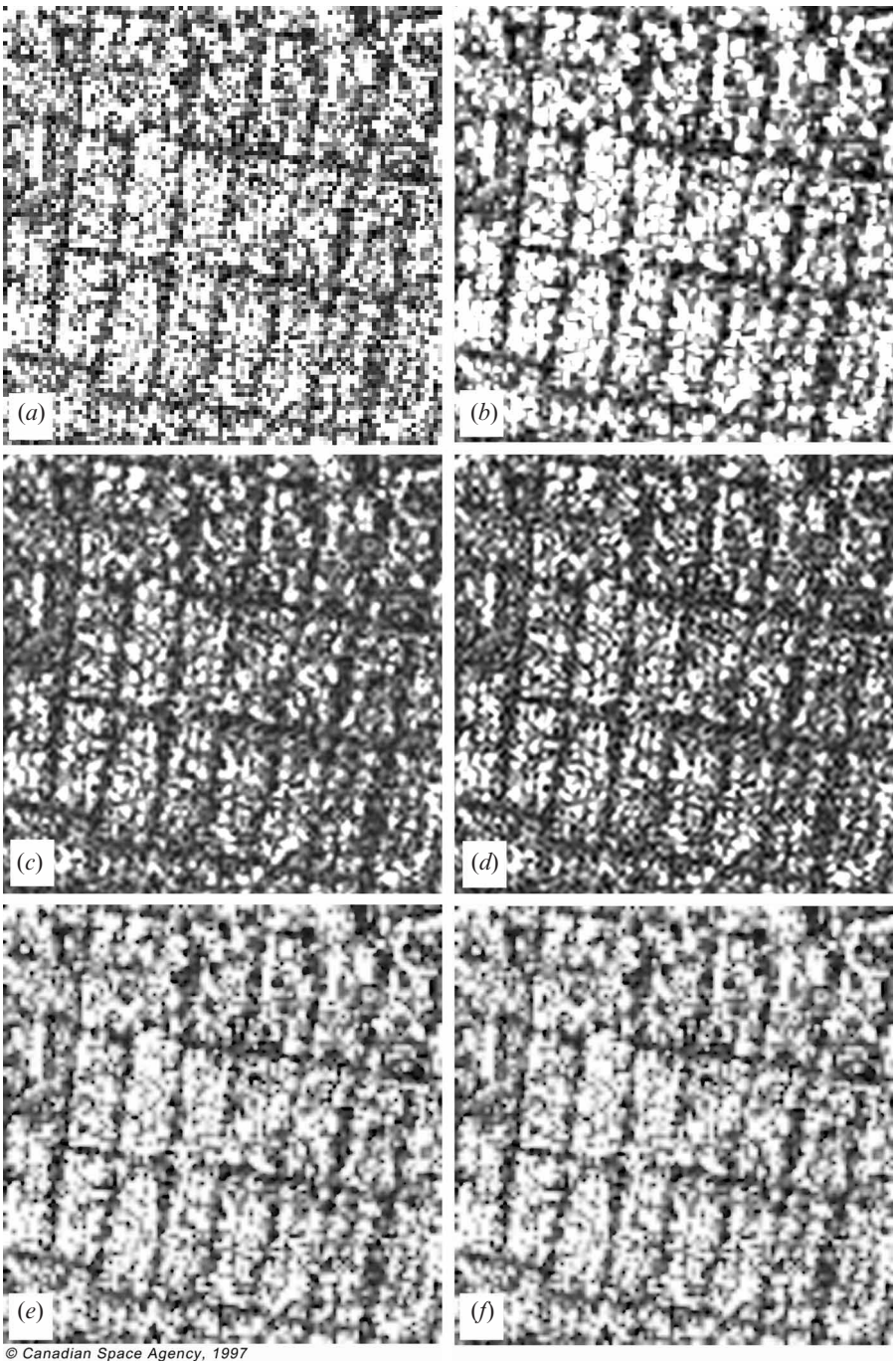


Figure 8. Examples of applications of geometric resampling kernels used in the rectification process with RADARSAT-SAR fine mode (F5) image. The sub-images are 600 by 600 pixels with 1.00-m spacing. Letters A, B, C and D refer to different geometric resampling kernels (nearest neighbour, bilinear, cubic convolution, $\sin(x)/x$ with $16 \times 16$ window), respectively and letters E and F refer to statistical SAR filters (Enhanced Lee and Gamma), respectively. RADARSAT Images © Canadian Space Agency, 2001.

window can be perceived on the car underneath while only the windshield is visible on the other car. It helps to differentiate a car and a station wagon! For the SAR image (figure 8), the two filters (E and F) give even better image appearance than the sinusoidal resampling, due to the fact that the SAR speckle is filtered at the same time.

## 5. Concluding remarks

Since the launch of the first civilian remote sensing satellite in the 1970s, the needs and requirements for geometrically processed remote sensing images have drastically changed. Furthermore, the integration of multi-format data in a digital world requires the highest accuracy possible so as to perform the ortho-rectification of multi-sensor images. For the last twenty years, two mathematical solutions have been developed for the geometric processing of remote sensing images: the physical and empirical models.

The major advantages of physical modelling over empirical modelling is mainly due to the fact that the mathematical functions correspond to the physical reality of the viewing geometry and take into account all the distortions generated in the image formation, while empirical model parameters do not have any physical meaning (Madani 1999, Dowman and Dolloff 2000). When the parameters have a physical meaning, bad or erroneous results are easy to find and interpret. Previous research studies with low/medium-resolution images (Salamonowicz 1986, Novak 1992, Toutin 1995a, de Sève *et al*. 1996), review papers and books (Konecny 1979, Wiesel 1984, Leberl 1990, Bannari *et al*. 1995, Caloz and Collet 2001) are all in agreement with these above statements. In addition, Dowman and Dolloff (2000) mentioned that there is no unanimity on the role for RFs to be adopted as a universal standard, and that the consensus seems to be in favour of rigorous physical models, but that RFs may be sometimes inevitable for some sensors. In other words, 3D physical and deterministic models should be the primary choice whenever available. In fact, the mathematical parameterization of physical and deterministic models has always been a major issue in scientific research and achievement.

## References

ACKERMAN, F., FRITSCH, D., HAHN, M., SCHNEIDER, F., and TSINGAS, V., 1995, Automatic generation of digital terrain models with MOMS-02/D2 data. *Proceedings of the MOMS-02 Symposium*, Köln, Germany, July 5–7 (Paris, France: EARSeL), pp. 79–86.

AHN, C.-H., CHO, S.-I., and JEON, J. C., 2001, Orthorectification software applicable for IKONOS high-resolution images: GeoPixel-Ortho. *Proceedings of IGARSS*, Sydney, Australia, July 9–13 2001 (Piscataway, NJ, USA: IEEF), pp. 555–557.

AL-ROUSSAN, N., CHENG, P., PETRIE, G., TOUTIN, TH., and VALADAN ZOEJ, M. J., 1997, Automated DEM extraction and ortho-image generation from SPOT level-1B imagery. *Photogrammetric Engineering and Remote Sensing*, **63**, 965–974.

BAETSLÉ, P. L., 1966, Conformal transformations in three dimensions. *Photogrammetric Engineering*, **32**, 816–824.

BÄHR, H. P., 1976, Geometrische Modelle für Abtasteraufzeichnungen von Erkundungd-satelliten. *Bildmessung und Luftbildwesen*, **44**, 198–202.

BALTSAVIAS, E. P., and STALLMANN, D., 1992, Metric information extraction from SPOT images and the role of polynomial mapping functions. *International Archives of Photogrammetry and Remote Sensing*, **29**, 358–364.

BANNARI, A., MORIN, D., BÉNIÉ, G. B., and BONN, F. J., 1995, A Theoretical review of different mathematical models of geometric corrections applied to remote sensing images. *Remote Sensing Reviews*, **13**, 27–47.

BELGUED, Y., GOZE, S., PLANÈS, J.-P., and MARTHON, PH., 2000, Geometrical Block Adjustment of Multi-Sensor Radar Images. *Proceedings of EARSeL Workshop: Fusion of Earth Data*, Sophia-Antipolis, France, January 26–28 (Nice, France: SEE GréCA/EARSeL), pp. 11–16.

BILLINGSLEY, F. C., 1983, Data processing and reprocessing. In *Manual of Remote Sensing*, 2nd edn, Vol. 1, edited by R. N. Colwell (Falls Church, Virginia, USA: Sheridan Press), pp. 719–722.

BONNEVAL, H., 1972, Levés topographiques par photogrammétrie aérienne. In *Photogrammétrie générale: Tome 3*, Collection scientifique de l'Institut Géographique National (Paris, France: Eyrolles Editeur).

BOUILLON, A., BRETON, E., DE LUSSY, F., and GACHET, R., 2002, SPOT5 HRG and HRS first in-flight geometric quality results. *Proceedings of SPIE, Vol. 4881A: Sensors, system, and Next Generation Satellites VII*, Agia Pelagia, Crete, Greece, 22–27 September 2002 (Bellingham, WA: SPIE), CD-ROM (Paper 4881A–31).

CALOZ, R., and COLLET, C., 2001, *Précis de télédétection* Transformations géométriques, In *Traitements numériques d'images de télédétection*, Volume 3 (Ste Foy, Québec, Canada: Presse de l'Université du Québec), pp. 76–105.

CAMPAGNE, PH., 2000, Apport de la spatio-triangulation pour la caractérisation de la qualité image géométrique. *Bulletin de la Société Française de Photogrammétrie et de Télédétection*, **159**, 66–26.

CANTOU, P., 2002, French Guiana mapped using ERS-1 radar imagery. Website of SPOT-Image, Toulouse, France (last accessed 15 November 2002; http://www.spotimage.fr/home/appli/apcarto/guiamap/welcome.htm).

CENTRE NATIONAL D'ÉTUDES SPATIALES (CNES), 1980, *Le mouvement du véhicule spatial en orbite* (Toulouse, France: CNES).

CHEN, L.-C., and TEO, T.-A., 2002, Rigorous generation of orthophotos from EROS-A high resolution satellite images. *International Archives of Photogrammetry and Remote Sensing and Spatial Information Sciences*, Ottawa, Canada, July 8–12 (Natural Resources Canada: Ottawa, Ontario) Vol. 34 (B4), pp. 620–625.

CHENG, P., and TOUTIN, T., 1998, Unlocking the potential for IRS-1C data. *Earth Observation Magazine*, **7**(3), 24–26.

CURLANDER, J. C., 1982, Location of spaceborne SAR imagery. *IEEE Transactions of Geoscience and Remote Sensing*, **22**, 106–112.

DAVIES, C. H., and WANG, X., 2001, Planimetric accuracy of IKONOS 1-m panchromatic image products. *Proceedings of the ASPRS Annual Conference*, St Louis, Missouri, USA, 23–27 April 2001 (ASPRS: Bethesda, USA), CD-ROM (unpaginated).

DE LEEUW, A. J., VEUGEN, L. M. M., and VAN STOKKOM, H. T. C., 1988, Geometric correction of remotely-sensed imagery using ground control points and orthogonal polynomials. *International Journal of Remote Sensing*, **9**, 1751–1759.

DE MASSON D'AUTUME, G., 1979, Le traitement géométrique des images de télédétection. *Bulletin de la Société Française de Photogrammétrie et de Télédétection*, **73–74**, 5–16.

DERENYI, E. E., 1970, An exploratory investigation into the relative orientation of continuous strip imagery. Research Report No. 8, University of New Brunswick, Canada.

DERENYI, E. E., and KONECNY, G., 1966, Infrared scan geometry. *Photogrammetric Engineering*, **32**, 773–778.

DE SÈVE, D., TOUTIN, T., and DESJARDINS, R., 1996, Evaluation de deux méthodes de corrections géométriques d'images Landsat-TM et ERS-1 RAS dans une étude de linéaments géologiques. *International Journal of Remote Sensing*, **17**, 131–142.

DIAL, G., and GRODECKI, J., 2002, Block adjustment with rational polynomial camera models. *Proceedings of the ACSM-ASPRS Annual Conference/XXII FIG International Congress*, Washington, DC, USA, 19–26 April 2002 (Bethesda, MD: ASPRS), CD-ROM.

DOWMANN, I., and DOLLOFF, J., 2000, An evaluation of rational function for photogrammetric restitution. *International Archives of Photogrammetry and Remote Sensing*, Amsterdam, The Netherlands, 16–23 July 2000 (Amsterdam, The Netherlands: GITC) Vol 33 (B3), pp. 254–266.

EBNER, H., and MULLER, F., 1986, Processing of digital three line imagery using a generalized model for combined point determination. *International Archives of Photogrammetry and Remote Sensing*, Rovamieni, Finland, 19–22 August (Finland: ISPRS) Vol. 26 (B3), pp. 212–222.

ESCOBAL, P. R., 1965, *Methods of orbit determination* (Malabar, USA: Krieger Publishing Company).

FRASER, C. S., HANLEY, H. B., and YAMAKAWA, T., 2002a, Three-dimensional geopositioning accuracy of IKONOS imagery. *Photogrammetric Record*, **17**, 465–479.

FRASER, C. S., BALTSAVIAS, E., and GRUEN, A., 2002b, Processing of IKONOS imagery for sub-metre 3D positioning and building extraction. *ISPRS Journal of Photogrammetry and Remote Sensing*, **56**, 177–194.

FRIEDMANN, D. E., FRIEDEL, J. P., MAGNUSSES, K. L., KWOK, K., and RICHARDSON, S., 1983, Multiple scene precision rectification of spaceborne imagery with few control points. *Photogrammetric Engineering and Remote Sensing*, **49**, 1657–1667.

GANAS, A., LAGIOS, E., and TZANNETOS, N., 2002, An investigation into the spatial accuracy of the IKONOS-2 orthoimagery within an urban environment. *International Journal of Remote Sensing*, **23**, 3513–3519.

GIBSON, J., 1984, Processing stereo imagery from line imagers. *Proceedings of 9th Canadian Symposium on Remote Sensing*, St. John's, Newfoundland, Canada, August 14–17 (Ottawa, Canada: Canadian Society for Remote Sensing), pp. 471–488.

GOPALA KRISHNA, B., KARTIKEYAN, B., IYER, K. V., REBANTREA MITRA, and SRIVASTAVA, P. K., 1996, Digital photogrammetric workstation for topographic map updating using IRS-1C stereo imagery. *International Archives of Photogrammetry and Remote Sensing*, Vienna, Austria, 9–18 July 1996 (Vienna, Austria: Austrian Society for Surveying and Geoinformation), Vol. 31, No. B4, pp. 481–485.

GOSHTASBY, A., 1988, Registration of Images with Geometric Distortions. *IEEE Transactions on Geoscience and Remote Sensing*, **26**, 60–64.

GRACIE, G., BRICKER, J. W., BREWER, R. K., and JOHNSON, R. A., 1970, Stereo radar analysis. US Engineer Topographic Laboratory, Report No. FTR-1339-1, Ft. Belvoir, VA, USA.

GRODECKI, J., 2001, IKONOS Stereo feature extraction—RPC approach. *Proceedings of the ASPRS Annual Conference*, St Louis, Missouri, USA, 23–27 April 2001 (Bethesda, MD: ASPRS), CD-ROM (unpaginated).

GUERTIN, F., and SHAW, E., 1981, Definition and potential of geocoded satellite imagery products. *Proceedings of the 7th Canadian Symposium on Remote Sensing*, Winnipeg, Canada, 8–11 September 1981 (Winnipeg, Canada: Manitoba Remote Sensing Centre), pp. 384–394.

GUGAN, D. J., 1987, Practical aspects of topographic mapping from SPOT imagery. *Photogrammetric Record*, **12**, 349–355.

GUICHARD, H., 1983, Etude théorique de la précision dans l'exploitation cartographique d'un satellite à défilement: application à SPOT. *Bulletin de la Société Française de Photogrammétrie et de Télédétection*, **90**, 15–26.

GUINDON, B., and ADAIR, M., 1992, Analytic formulation of spaceborne SAR image geocoding and value-added products generation procedures using digital elevation data. *Canadian Journal of Remote Sensing*, **18**, 2–12.

HANLEY, H. B., and FRASER, C. S., 2001, Geopositioning accuracy of IKONOS imagery: Indications from two dimensional transformations. *Photogrammetric Record*, **17**, 317–329.

HARGREAVES, D., and ROBERTSON, B., 2001, Review of Quickbird-1/2 and Orbview-3/4 products from MacDonald Dettwiler Processing Systems. *Proceedings of the ASPRS Annual Conference*, St Louis, Missouri, USA, 23–27 April 2001 (Bethesda, MD: ASPRS), CD-ROM (unpaginated).

HOFFMANN, O., and MULLER, F., 1988, Combined point determination using digital data of three line scanner systems. *International Archives of Photogrammetry and Remote Sensing*, Kyoto, Japan, 3–9 July 1988 (Japan: ISPRS), Vol. 27 (B3), pp. 567–577.

HOFFMANN, C., STEINNOCHER, K., KASANKO, M., TOUTIN, T., and CHENG, P., 2001, Urban mapping with high resolution satellite imagery: IKONOS and IRS data put to the test. *GeoInformatics*, **4**, 34–37.

HOOGEBOOM, P., BINNENKADE, P., and VEUGEN, L. M. M., 1984, An algorithm for radiomeric and geometric correction of digital SLAR data. *IEEE Transactions on Geoscience and Remote Sensing*, **22**, 570–576.

JACOBSEN, K., 1997, Calibration of IRS-1C Pan camera. *ISPRS Workshop on Sensors and Mapping from Space*, Hannover, Germany, 29 September–2 October (Bonn,

Germany: German Society for Photogrammetry and Remote Sensing/ISPRS), pp. 163–170.

JACOBSEN, K., 2002, Generation of orthophotos with Carterra Geo images without orientation information. *Proceedings of the ACSM-ASPRS Annual Conference/XXII FIG International Congress*, Washington DC, USA, 19–26 April 2002 (Bethesda, MD: ASPRS), CD-ROM (unpaginated).

KALMAN, L. S., 1985, Comparison of cubic-convolution interpolation and least-squares restoration for resampling Landsat-MSS imagery. *Proceedings of the 51st Annual ASP-ASCM Convention: 'Theodolite to Satellite'*, Washington DC, USA, March 10–15 (Falls Church, VA: ASP), pp. 546–556.

KERSTEN, T., BALTSAVIAS, E., SCHWARZ, M., and LEISS, I., 2000, Ikono-2 Cartera Geo – Erste geometrische Genauigkeitsuntersuchungen in der Schweiz mit hochaufgeloesten Satellitendaten. *Vermessung, Photogrammetrie, Kulturtechnik*, **8**, 490–497.

KHIZHNICHENKO, V. I., 1982, Co-ordinates transformation when geometrically correcting Earth space scanner images. *Earth Exploration From Space*, **5**, 96–103 (in Russian).

KIM, J. R., and MULLER, J.-P., 2002, 3D reconstruction from very high resolution satellite stereo and its application to object identification. *International Archives of Photogrammetry and Remote Sensing and Spatial Information Sciences*, Ottawa, Canada, July 8–12 (Ottawa, Ontario: Natural Resources Canada), Vol. 34 (B4), pp. 637–643.

KONECNY, G., 1970, Metric problems in remote sensing. *ITC Publications Series A*, **50**, 152–177.

KONECNY, G., 1976, Mathematische Modelle und Verfahren zur geometrischen Auswertung von Zeilenabtaster-Aufnahmen. *Bildmessung und Luftbildwesen*, **44**, 188–197.

KONECNY, G., 1979, Methods and possibilities for digital differential rectification. *Photogrammetric Engineering and Remote Sensing*, **45**, 727–734.

KONECNY, G., KRUCK, E., and LOHMANN, P., 1986, Ein universeller Ansatz für die geometrischen Auswertung von CCD-Zeilenabtasteraufnahmen. *Bildmessung und Luftbildwesen*, **54**, 139–146.

KONECNY, G., LOHMANN, P., ENGEL, H., and KRUCK, E., 1987, Evaluation of SPOT imagery on analytical instruments. *Photogrammetric Engineering and Remote Sensing*, **53**, 1223–1230.

KORNUS, W., LEHNER, M., and SCHROEDER, M., 2000, Geometric in-flight calibration by block adjustment using MOMS-2P 3-line-imagery of three intersecting stereo-strips. *Bulletin de la Société Française de Photogrammétrie et de Télédétection*, **159**, 42–54.

KRATKY, W., 1971, Precision processing of ERTS imagery. *Proceedings of ASP-ACSM Fall Convention*, San Fransisco, CA, 7–11 September 1971 (Falls Church, VA: ASP) pp. 481–514.

KRATKY, W., 1987, Rigorous stereophotogrammetric treatment of SPOT images. *Comptes-rendus du Colloque International sur SPOT-1: utilisation des images, bilans, résultats*, Paris, France, November 1987 (Toulouse, France: CEPADUES), pp. 1281–1288.

KRATKY, W., 1989, On-line aspects of stereophotogrammetric processing of SPOT images. *Photogrammetric Engineering and Remote Sensing*, **55**, 311–316.

KRISTÓF, D., CSATÓ, É., and RITTER, D., 2002, Application of high-resolution satellite images in forestry and habitat mapping – evaluation of IKONOS images through a Hungarian case study. *International Archives of Photogrammetry and Remote Sensing and Spatial Information Sciences*, Ottawa, Canada, 8–12 July 2002 (Natural Resources Canada: Ottawa, Ontario), Vol. 34 (B4), pp. 602–607.

LA PRADE, G. L., 1963, An analytical and experimental study of stereo for radar. *Photogrammetric Engineering*, **29**, 294–300.

LEBERL, F. W., 1972, On model formation with remote sensing imagery. *Österreichiches Zeitschrift für Vermessungswesen*, **2**, 43–61.

LEBERL, F. W., 1978, Satellite radargrammetric. *Deutsche Geodactische Kommission*, Munich, Germany, Serie C, 239.

LEBERL, F. W., 1990, *Radargrammetric image processing* (Norwood, USA: Artech House).

LEE, J.-B., HUH, Y., SEO, B., and KIM, Y., 2002, Improvement the positional accuracy of the 3D terrain data extracted from IKONOS-2 satellite imagery. *International Archives of Photogrammetry and Remote Sensing*, Graz, Austria, September 9–13 (Institute for Computer Graphics and Vision: Graz, Austria), Vol. 34 (B3), pp. B142–B145.

LEE, J. S., 1980, Digital image enhancement and noise filtering by use of local statistics. *IEEE Transactions on Pattern Analysis and Machine Intelligence*, **2**, 165–168.

LIGHT, D. L., BROWN, D., COLVOCORESSES, A., DOYLE, F., DAVIES, M., ELLASAL, A., JUNKINS, J., MANENT, J., MCKENNEY, A., UNDREJKA, R., and WOOD, G., 1980, Satellite photogrammetry. In *Manual of Photogrammetry* 4th edn, edited by C. C. Slama (Falls Church, USA: ASP Publishers), pp. 883–977.

LOPES, A., NEZRY, E., TOUZI, R., and LAUR, H., 1993, Structure detection and statistical adaptive speckle filtering in SAR images. *International Journal of Remote Sensing*, **14**, 1735–1758.

MADANI, M., 1999, Real-time sensor-independent positioning by rational functions. *Proceedings of ISPRS Workshop on Direct Versus Indirect Methods of Sensor Orientation*, Barcelona, Spain, 25–26 November 1999 (Barcelona, Spain: ISPRS), pp. 64–75.

MCCARTHY, F., CHENG, P., and TOUTIN, T., 2001, Case study of using IKONOS imagery in small municipalities. *Earth Observation Magazine*, **10**(11), 13–16.

MEINEL, G., and REDER, J., 2001, IKONOS Satellitenbilddaten—ein erster Erfahrungsbericht. *Kartographische Nachrichten*, **51**, 40–46.

MIKHAIL, E. M., 1976, *Observations and Least Squares* (New York USA: Harper & Row Publishers).

NARAGHI, M., STROMBERG, W., and DAILY, M., 1983, Geometric rectification of radar imagery using digital elevation models. *Photogrammetric Engineering and Remote Sensing*, **49**, 195–159.

OGC, 1999, *The Open GISTM Abstract Specifications: The Earth Imagery Case*, Vol. 7, http://www.opengis.org/techno/specs/htm/.

OKAMOTO, A., 1981, Orientation and construction of models. Part III: Mathematical Basis of the orientation problem of one-dimensional central perspective photographs. *Photogrammetric Engineering and Remote Sensing*, **47**, 1739–1752.

OKAMOTO, A., 1988, Orientation theory of CCD line-scanner images. *International Archives of Photogrammetry and Remote Sensing*, Kyoto, Japan, 3–9 July 1988 (Japan: ISPRS) Vol. 27 (B3), pp. 609–617.

OKAMOTO, A., FRASER, C., HATTORI, S., HASEGAWA, H., and ONO, T., 1998, An alternative approach to the triangulation of SPOT imagery. *International Archives of Photogrammetry and Remote Sensing*, Stuttgart, Germany, September 7–10 (Stuttgart: German Society for Photogrammetry and Remote Sensing), Vol. 32 (B4), pp. 457–462.

PADERES, F. C., MIKHAIL, E. M., and FAGERMAN, J. A., 1989, Batch and on-line evaluation of stereo SPOT imagery. *Proceedings of the ASPRS – ACSM Convention*, Baltimore, MD (Bethesda, MD: ASPRS), Vol. 3, pp. 31–40.

PALÀ, V., and PONS, X., 1995, Incorporation of relief in polynomial-based geometric corrections. *Photogrammetric Engineering and Remote Sensing*, **61**, 935–944.

PETRIE, G., 2002, The ACSM-ASPRS Conference: A report on the Washington meeting. *GeoInformatics*, **5**, 42–43.

ROBERTSON, B., ERICKSON, A., FRIEDEL, J., GUINDON, B., FISHER, T., BROWN, R., TEILLET, P., D'IORIO, M., CIHLAR, J., and SANZ, A., 1992, GeoComp, a NOAA AVHRR geocoding and compositing system. *International Archives of Photogrammetry and Remote Sensing*, Washington DC, 3–14 August 1992 (Bethesda, MD: ASPRS) Vol. 24 (B2), pp. 223–228.

ROSENFIELD, G. H., 1968, Stereo radar techniques. *Photogrammetric Engineering*, **34**, 586–594.

SAKAINO, S., SUZUKI, H., CHENG, P., and TOUTIN, T., 2000, Updating maps of Kazakhstan using stitched SPOT images. *Earth Observation Magazine*, **9**(3), 11–13.

SALAMONOWICZ, P. H., 1986, Satellite Orientation and position for geometric correction of scanner imagery. *Photogrammetric Engineering and Remote Sensing*, **52**, 491–499.

SAVOPOL, F., LECLERC, A., TOUTIN, TH., and CARBONNEAU, Y., 1994, La correction géométrique d'images satellitaires pour la Base nationale de données topographiques. *Geomatica, été*, **48**, 193–207.

SAWADA, N., KIKODE, M., SHINODA, H., ASADA, H., IWANAGA, M., WATANABE, S., and MORI, K., 1981, An analytic correction method for satellite MSS geometric distortion. *Photogrammetric Engineering and Remote Sensing*, **47**, 1195–1203.

SCHUT, G. H., 1966, Conformal transformations and polynomials. *Photogrammetric Engineering*, **32**, 826–829.

SHU, N., 1987, Restitution géométrique des images spatiales par la méthode de l'équation de

colinéarité. *Bulletin de la Société Française de Photogrammétrie et de Télédétection*, **105**, 27–40.

SYLVANDER, S., HENRY, P., BASTIEN-THIERY, C., MEUNIER, F., and FUSTER, D., 2000, Vegetation geometrical image quality. *Bulletin de la Société Française de Photogrammétrie et de Télédétection*, **159**, 59–65.

TANNOUS, I., and PIKEROEN, B., 1994, Parametric modelling of spaceborne SAR image geometry. Application: SEASAT/SPOT image registration. *Photogrammetric Engineering and Remote Sensing*, **60**, 755–766.

TAO, V., and HU, Y., 2001, A comprehensive study of the rational function model for photogrammetric processing. *Photogrammetric Engineering and Remote Sensing*, **67**, 1347–1357.

TAO, V., and HU, Y., 2002, 3D reconstruction methods based on the rational function model. *Photogrammetric Engineering and Remote Sensing*, **68**, 705–714.

TOUTIN, T., 1983, Analyse mathématique des possibilités cartographiques du satellite SPOT. *Mémoire du diplôme d'Etudes Approfondies*, Ecole Nationale des Sciences Géodésiques Saint-Mandé, France, pp. 1–74.

TOUTIN, T., 1985, Analyse mathématique des possibilités cartographiques de système SPOT. *Thèse de Docteur-Ingénieur*, École Nationale des Sciences Géodésiques (St-Mandé, France: IGN).

TOUTIN, T., 1995a, Intégration de données multi-sources : comparaison de méthodes géométriques et radiométriques. *International Journal of Remote Sensing*, **16**, 2795–2811.

TOUTIN, T., 1995b, Multi-source Data integration with an integrated and unified geometric modelling. *EARSeL Journal Advances in Remote Sensing*, **4**, 118–129.

TOUTIN, T., 1998, Evaluation de la précision géométrique des images de RADARSAT. *Journal canadien de télédétection*, **24**, 80–88.

TOUTIN, T., 1999, Error tracking of radargrammetric DEM from RADARSAT images. *IEEE-Transactions on Geoscience and Remote Sensing*, **37**, 2227–2238.

TOUTIN, T., 2003b, Block bundle adjustment of Ikonos in-track images. *International Journal of Remote Sensing*, **24**, 851–857.

TOUTIN, T., 2003a, Error tracking in IKONOS geometric processing using a 3D parametric modelling. *Photogrammetric Engineering and Remote Sensing*, **69**, 43–51.

TOUTIN, T., 2003c, Block bundle adjustment of Landsat7 $ETM^+$ images over mountainous areas. *Photogrammetic Engineering and Remote Sensing*, **69**, accepted.

TOUTIN, T., 2003d, Path processing and block adjustment with RADARSAT-1 SAR images. *IEEE Transactions on Geoscience and Remote Sensing*, **40**, in press.

TOUTIN, T., and CARBONNEAU, Y., 1992, MOS and SEASAT image geometric corrections. *IEEE Transactions on Geoscience and Remote Sensing*, **30**, 603–609.

TOUTIN, T., and CHENG, P., 2000, Demystification of IKONOS. *Earth Observation Magazine*, **9**(7), 17–21.

TOUTIN, T., and CHENG, P., 2002, QuickBird: A milestone to high resolution mapping. *Earth Observation Magazine*, **11**(4), 14–18.

TOUTIN, T., CARBONNEAU, Y., and St. LAURENT, L., 1992, An integrated method to rectify airborne radar imagery using DEM. *Photogrammetic Engineering and Remote Sensing*, **58**, 417–422.

TOUTIN, T., CHÉNIER, R., and CARBONNEAU, Y., 2002, 3D models for high resolution images: examples with QuickBird, IKONOS and EROS. *Proceedings of Joint International Symposium on Geospatial Theory, Processing and Applications (ISPRS, IGU, CIG)*, Ottawa, Ontario, Canada, 8–12 July 2002, CD-ROM.

TOUZI, R., 2002, A review of speckle filtering in the context of estimation theory. *IEEE Transactions on Geoscience and Remote Sensing*, **40**, in press.

VALADAN ZOEJ, M. J., and PETRIE, G., 1998, Mathematical modelling and accuracy testing of SPOT Level-1B stereo-pairs. *Photogrammetric Record*, **16**, 67–82.

VALADAN ZOEJ, M. J., MANSOURIAN, A., MOJARADI, B., and SADEGHIAN, S., 2002, 2D geometric correction of IKONOS imagery using genetic algorithm. *International Archives of Photogrammetry and Remote Sensing and Spatial Information Sciences*, Vol. 34 (B4), CD-ROM (unpaginated).

VASSILOPOULOU, S., HURNI, L., DIETRICH, V., BALTSAVIAS, E., PATERAKI, M., LAGIOS, E., and PARCHARIDIS, I., 2002, Orthophoto generation using IKONOS imagery and

high-resolution DEM: a case study on volcanic hazard monitoring of Nisyros Island (Greece). *ISPRS Journal of Photogrammetry and Remote Sensing*, **57**, 24–38.

VEILLET, I., 1991, Triangulation spatiale de blocs d'images SPOT. *Thèse de Doctorat*, Observatoire de Paris, Paris, France.

WESTIN, T., 1990, Precision rectification of SPOT imagery. *Photogrammetric Engineering and Remote Sensing*, **56**, 247–253.

WESTIN, T., 2000, Geometric modelling of imagery from the MSU-SK conical scanner. *Société Française de Photogrammétrie et de Télédétection*, **159**, 55–58.

WESTIN, T., and FORSGREN, J., 2002, Orthorectification of EROS-A1 images. *ImageSat International website* (last accessed 20 April 2003; http://www.imagesatintl.com/customers/techarticles/Orthorectification_EROSA1Images.pdf).

WIESEL, J. W., 1984, Image rectification and registration. *International Archives of Photogrammetry and Remote Sensing*, Rio de Janeiro, Brazil (Brazil: ISPRS), Vol. 25 (A3b), pp. 1120–1129.

WONG, K. W., 1975, Geometric and cartographic accuracy of ERTS-1 imagery. *Photogrammetric Engineering and Remote Sensing*, **41**, 621–635.

WONG, K. W., 1980, Basic mathematics of photogrammetry. In *Manual of Photogrammetry*, 4th edn, edited by C. C. Slama (Falls Church, USA: ASP Publishers), pp. 37–101.

WONG, F., ORTH, R., and FRIEDMANN, D., 1981, The use of digital terrain model in the rectification of satellite-borne imagery. *Proceedings of the 15th International Symposium on Remote Sensing of Environment*, Ann Arbor, Michigan, May 11–15 (ERIM: Ann Arbor, USA), pp. 653–662.

YANG, X., 2001, Piece-wise linear rational function approximation in digital photogrammetry. *Proceedings of the ASPRS Annual Conference*, St Louis, Missouri, USA, April 23–27 2001 (ASPRS: Bethesda, USA), CD-ROM (unpaginated).

ZHANG, Y., TAO, V., and MERCER, B., 2001, Assessment of the influences of satellite viewing angle, Earth curvature, relief height, geographical location and DEM characteristics on planimetric displacement of high-resolution satellite imagery. *Proceedings of the ASPRS Annual Conference*, St Louis, Missouri, April 23–27 2001 (ASPRS: Bethesda, USA), CD-ROM (unpaginated).